Resonance Frequencies and Q-factors of Multi-Resonance Complex Electromagnetic Systems

M. Dohlus[1], V. Kaljuzhny[2], S. G. Wipf[1]

[1]Deutsches Elektronen Synchrotron, DESY, Hamburg, Germany
[2]Moscow Engineering Physics Institute, MEPI, Moscow, Russia

Abstract

We present the calculation results for a lossless TTF cavity-coupler unit, for combination cavity-coupler units and for an 8-cavity accelerating module, at the frequency band corresponding to third dipole band of the 9-cell TTF cavity. Experimental investigations of the copper TESLA Test Facility cavity, equipped with two higher order mode couplers, are also presented, for the original and the modified ("mirrored") downstream higher order mode couplers.

Here we developed the procedure for the determination of resonant frequencies and Q-factors using the dependence of the complex transmission coefficient $S_{m,n}(f)$ or the complex reflection coefficient $S_{m,m}(f)$ on frequency in the frequency band under investigation. These dependencies were obtained from the numerical calculation of S-parameters of lossless TESLA Test Facility (TTF) modules in the third dipole mode frequency band and from the experimental investigation of the copper TESLA Test Facility cavity equipped with two higher order mode couplers in the first, second and third dipole mode frequency bands, second quadrupole and second monopole mode frequency band. The procedure permits us to determine resonant frequencies and Q-factors (Q_o, Q_{Load} and Q_{ext}) using a large enough frequency step (Δf) with only few frequency points located on the resonance curve corresponding to the high Q-factor resonance.

Contents

1. Introduction

The TTF 8-cavity accelerating module is a complex multi-resonance electromagnetic system. It consists of eight cavity-coupler units connected to each other by cylindrical 78-mm diameter bellows [1,2,3]. At the same time each cavity-coupler unit consists of a 9-cell TESLA cavity, upstream higher order mode coupler (HOMC) and downstream higher order mode coupler and fundamental mode coupler (HOMC+FMC). Fig.1 shows a schematic representation of the cavity-coupler unit in the frequency rang, corresponding to the 3rd dipole band of the TESLA cavity.

There are different types of HOMCs and FMCs [1,2,3]. Here we consider cavity-coupler units containing DESY-type HOMCs and DESY-II type FMCs shown in Fig.2 and Fig.3.

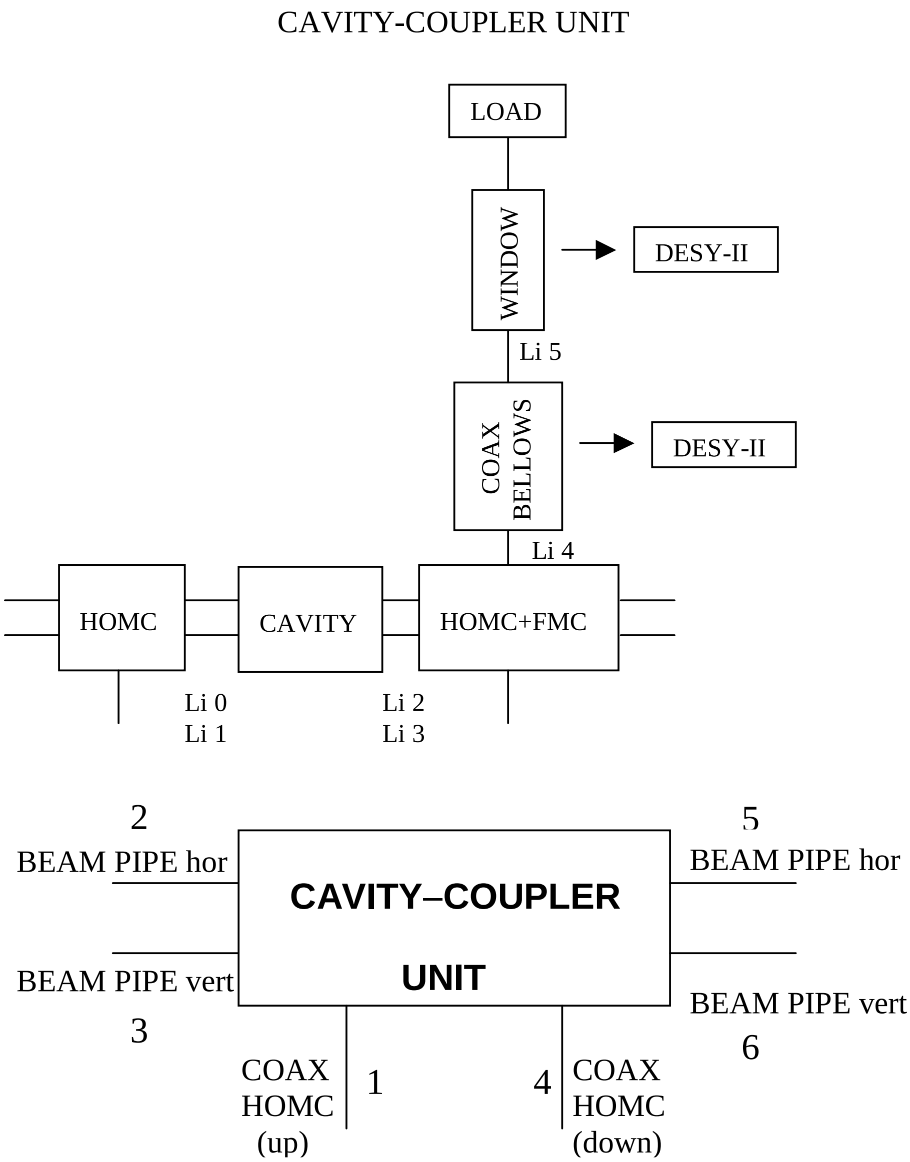

Fig.1. Schematic representation of the cavity-coupler unit.

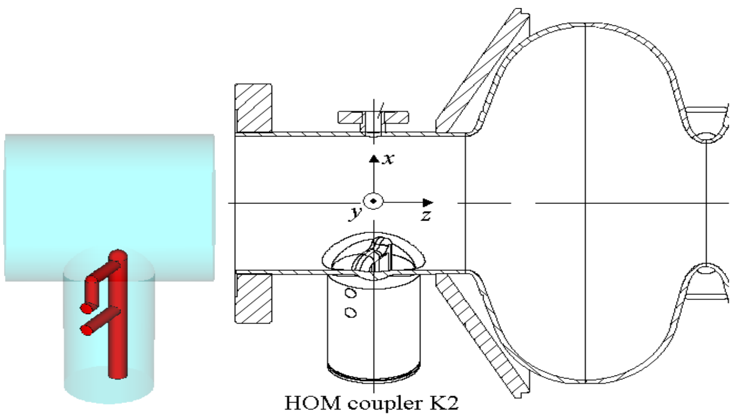

a)Upstream HOMC

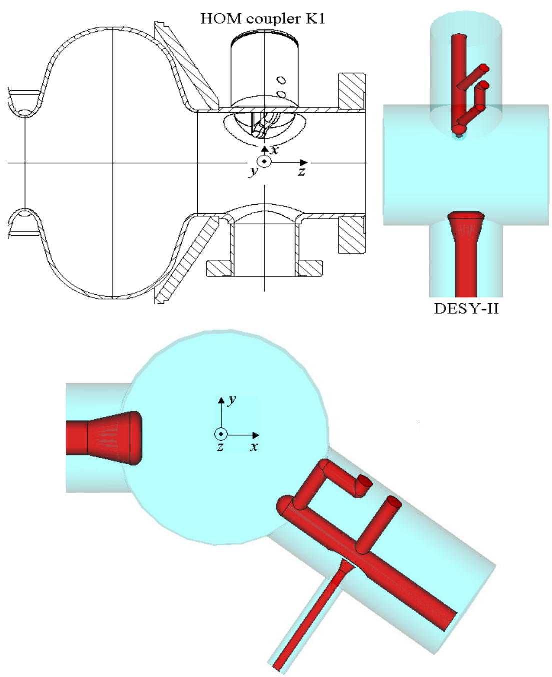

b) Down stream HOMC+FMC

Fig.2. Upstream (a) HOMC and downstream (b) HOMC+FMC.

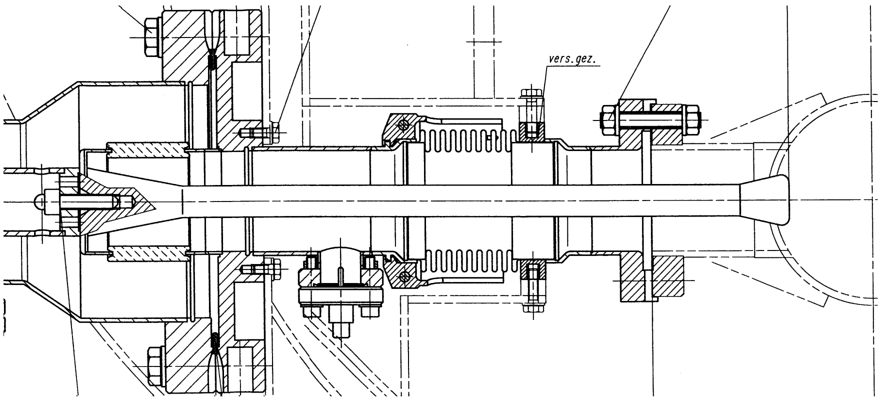

Fig.3. DESY-II type FMC

The cavity-coupler unit shown in Fig.1 is represented as a 6-port device. Port 1 and Port 4 correspond to coaxial output ports of the upstream and downstream HOMCs. Other ports (2,3,5,6) shown in the figure correspond to the double polarization of the dipole mode (HOM) in the beam-pipes. We call this double polarization horizontal and vertical polarization. Horizontal polarization corresponds to the x-axis (axis of the coaxial line of the FMC shown in Fig.2) and vertical polarization corresponds to the y-axis, the z-axis goes along the cavity axis. Ports 2 and 3 belong physically to the same left cylindrical beam-pipe while ports 5 and 6 belong to the right cylindrical beam-pipe. Such representation of the cavity-coupler unit is used to calculate S-parameters of the different sub-units (upstream HOMC as 5-port sub-unit, cavity as 4-port sub-unit, downstream HOM+FMC as 6-port sub-unit, coaxial bellows and cold window, shown in Fig.3 and Fig.1, as 2-port sub-units). As the reflection coefficient of the cold DESY-II window is very large in the 3rd dipole mode frequency band, the load is assumed to be matched.

Fig.4 shows schematic representation of the 8-cavity accelerating module. Here the cavity-coupler units are connected to each other by cylindrical 78-mm diameter bellows-beam-pipes. Four loads may be matched loads and/or may have any known input impedance (reflection coefficient). In this figure the 8-cavity accelerating module is represented as a 16-port device and is described by a 16×16 scattering matrix. Each port corresponds to coaxial output of upstream or downstream HOMC.

The detailed description of the S-parameter calculation for different sub-units can be found in [4], where the calculation for very complex units containing eight cavity-coupler units with varying parameters (for example cavity detuning or some changing in design of the different sub-units), is described.

Here we describe the procedure for the determination of resonant frequencies and Q-factors using the dependence of the complex transmission coefficient $S_{m,n}(f)$ or the complex reflection coefficient $S_{m,m}(f)$ on frequency in the frequency band under investigation. Some examples of such calculations are also presented. This procedure can be used in experimental investigation of the 8-cavity accelerating module under low temperature conditions.

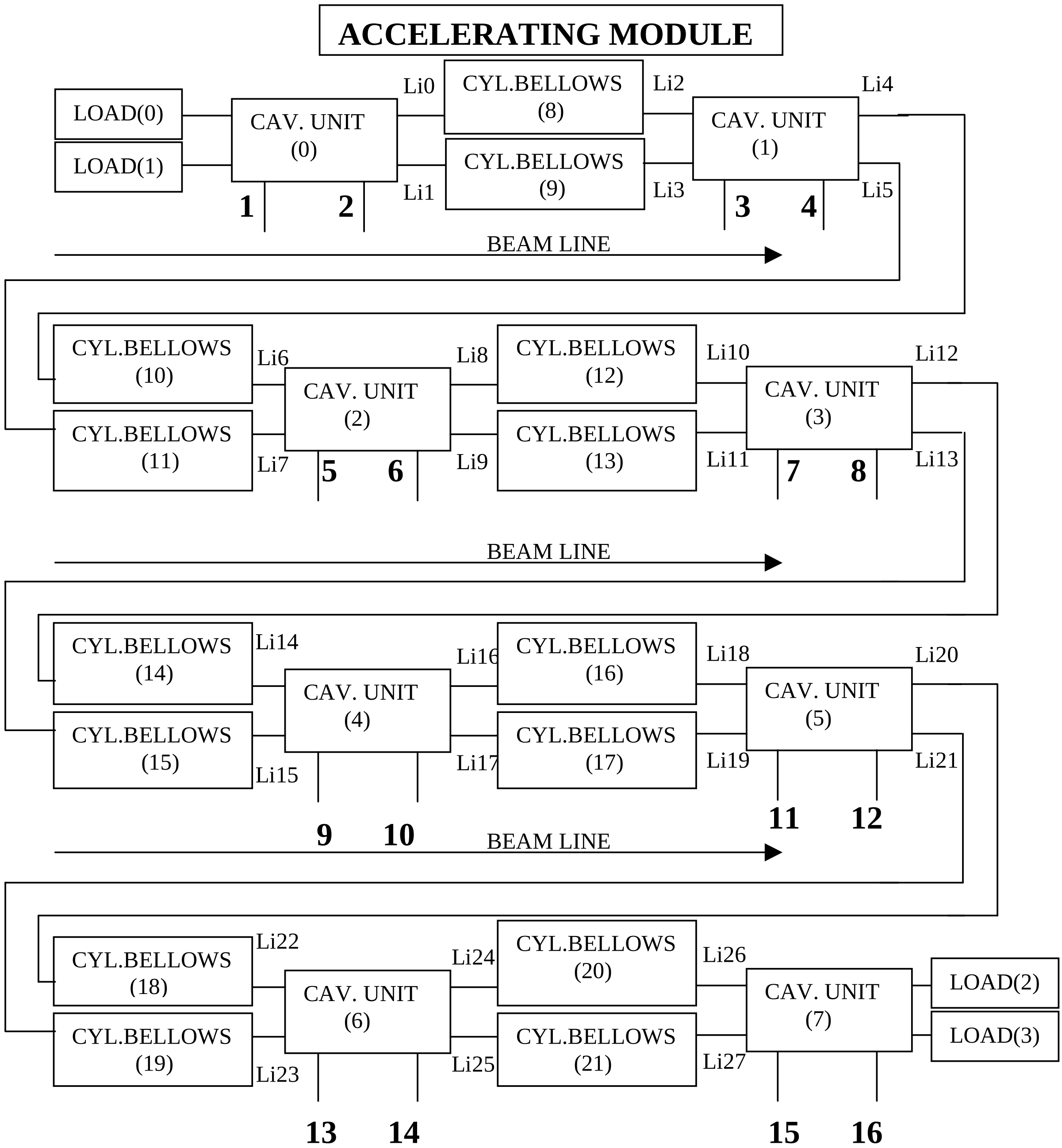

Fig.4. Schematic representation of the 8-cavity accelerating module.

2. Theoretical Basis

In our investigation we use the S-parameter concept described in [4]. As a result of either numerical calculation or measurement of the transmission coefficient $S_{m,n}$ ($m \neq n$) of a complex N-port device we obtain two arrays:

$f_i \Rightarrow f_1, f_2, \ldots, f_i, \ldots, f_I$ (frequency array, $i = 1, 2, 3, \ldots, I$),

$S_{m,n}(f_i) \Rightarrow S_{m,n}(f_1), S_{m,n}(f_2), \ldots, S_{m,n}(f_i), \ldots, S_{m,n}(f_I)$ (array of complex transmission coefficients at frequencies f_i, corresponding to ports m and n, other ports are terminated with matched loads).

This transmission coefficient dependence on frequency covers a frequency band from f_1 to f_I with a frequency step of Δf. The problem is to find all resonant frequencies $f_{o,k}$, $k = 1, 2, 3, \ldots, K$, and loaded Q-factors $Q_{Load,k}$ ($k = 1, 2, 3, \ldots, K$) corresponding to these resonant frequencies in the frequency band under investigation.

We approximate the transmission coefficient dependence on frequency with the following formula

$$S_{m,n\,app}(f) = \sum_{k=1}^{K} \frac{S_k}{1 + jQ_{Load,k}\left(\frac{f}{f_{o,k}} - \frac{f_{o,k}}{f}\right)} \qquad (1)$$

where $f_{o,k}$ is unknown resonant frequency (real value, $k = 1, 2, 3, \ldots, K$),

$Q_{Load,k}$ is unknown loaded Q-factor (real value, $k = 1, 2, 3, \ldots, K$),

S_k is unknown complex coefficient (complex value, $k = 1, 2, 3, \ldots, K$),

K is a number of resonant frequencies taken into account in the frequency band under investigation.

In the first step of calculation we choose zero order approximation for $f_{o,k}$ and $Q_{Load,k}$. Using the given transmission coefficient dependence on frequency $S_{m,n}(f_i)$ we can choose K frequencies $f_{i(k)}$, which are more or less close to resonant frequencies in the frequency band under investigation, where $i(k) = i(1), i(2), i(3), \ldots, i(K)$, $k = 1, 2, 3, \ldots, K$ and suppose $f_{o,k} = f_{i(k)}$. We can suppose $Q_{Load,k}$ equals some value taking into consideration the curve $S_{m,n}(f_i)$ plotted in the complex plane.

Then we introduce ERROR-function as follows

$$\text{ERROR} = \frac{1}{I}\sum_{i=1}^{I}\left| S_{m,n}(f_i) - \sum_{k=1}^{K} \frac{S_k}{1 + jQ_{Load,k}\left(\frac{f_i}{f_{o,k}} - \frac{f_{o,k}}{f_i}\right)} \right| \qquad (2)$$

The ERROR-function (2) is a function of 4K unknown real parameters ($f_{o,k}$, $Q_{Load,k}$, $Re(S_k)$ and $Im(S_k)$). To reduce the number of unknown parameters we can require that

$$S_{m,n}\left(f_{i(k)}\right) = \sum_{k=1}^{K} \frac{S_k}{1 + jQ_{Load,k}\left(\frac{f_{i(k)}}{f_{o,k}} - \frac{f_{o,k}}{f_{i(k)}}\right)} \quad \text{, for } i(k) = i(1), i(2), i(3), \dots, i(K)$$

and obtain the following set of linear equations for complex coefficients S_k

$$\sum_{k=1}^{K} A_{i,k} S_k = \sum_{k=1}^{K} \frac{S_k}{1 + jQ_{Load,k}\left(\frac{f_{i(k)}}{f_{o,k}} - \frac{f_{o,k}}{f_{i(k)}}\right)} = S_{m,n}\left(f_{i(k)}\right) \tag{3}$$

$$\text{for } i(k) = i(1), i(2), i(3), \dots, i(K)$$

So the curve described by the expression (1) and curve $S_{m,n}(f_i)$ plotted on the complex plane go through the same points corresponding to i(k) = i(1), i(2), i(3), … , i(K). Of course these two curves be very different in the other points due to the very rough estimation of the resonant frequencies ($f_{o,k}$) and loaded Q-factors ($Q_{Load,k}$).

Now we can consider the ERROR-function (2) as a function of only $f_{o,k}$ and $Q_{Load,k}$ (2K unknown parameters). In the next step we consider $f_{o,k}$ and $Q_{Load,k}$ as variable values and **minimize** the ERROR-function (2). To minimize ERROR-function we can use the following procedure. First we change only $f_{o,1}$ and $Q_{Load,1}$ (other $f_{o,k}$ and $Q_{Load,k}$ are fixed). Then we change only $f_{o,2}$ and $Q_{Load,2}$ and so on up to $f_{o,K}$ and $Q_{Load,K}$. This cycle can be repeated many times. After any changing in $f_{o,k}$ and/or $Q_{Load,k}$ we have to calculate the complex coefficients S_k using the set of equation (3). So in each step of minimization the ERROR-function is a function of only two variables. In the ideal case ERROR-function has minimum $ERROR_{min} = 0$.

If we know that investigated system has resonances outside the frequency band from f_1 to f_I we have to add one or two additional terms in the expressions (3) and (2) corresponding to i = 1 and/or i = I. These additional terms are required to replace resonances located outside the frequency band from f_1 to f_I (lower than f_1 and/or higher than f_I).

In the case of a loss-free device, the loaded Q-factor $Q_{Load,k}$ and external Q-factor $Q_{ext,k}$ are equal to each other ($Q_{Load,k} = Q_{ext,k}$) and Q_o-factor $Q_{o,k} = \propto$. But if the device has losses we have to find the external Q-factor $Q_{ext,k}$ and $Q_{o,k}$. To find these values we use the dependence on frequency of reflection coefficients $S_{m,m}(f_i)$ and $S_{n,n}(f_i)$ measured with Network Analyzer (NWA) and corresponding to ports m and n (other ports are terminated with matched loads).

We approximate the reflection coefficient dependence on frequency by the following formula (other ports are matched)

$$S_{m,m\,app}(f) = \sum_{k=1}^{K} \frac{\Gamma_{m,k} - jQ_{Load,k}\left(\frac{f}{f_{o,k}} - \frac{f_{o,k}}{f}\right)}{1 + jQ_{Load,k}\left(\frac{f}{f_{o,k}} - \frac{f_{o,k}}{f}\right)} \exp(j\psi_{m,k})$$

here $\Gamma_{m,k}$ is real unknown value ($-1 < \Gamma_{m,k} < +1$),

$\psi_{m,k}$ is real unknown value ($-\pi < \psi_{m,k} < +\pi$),

$f_{o,k}$ and $Q_{Load,k}$ are unknown values.

The last expression can be written in the following form

$$S_{m,m\,app}(f) = \sum_{k=1}^{K} \left\{ \frac{(\Gamma_{m,k} + 1)\exp(j\psi_{m,k})}{1 + jQ_{Load,k}\left(\frac{f}{f_{o,k}} - \frac{f_{o,k}}{f}\right)} - \exp(j\psi_{m,k}) \right\} \tag{4}$$

here $0 < \Gamma_{m,k} + 1 < +2$.

To determine $f_{o,k}$ and $Q_{Load,k}$ we minimize two error-functions

$$\begin{aligned} ERROR_m &= \frac{1}{I}\sum_{i=1}^{I} \left| S_{m,m}(f_i) - \sum_{k=1}^{K} \left\{ \frac{(\Gamma_{m,k} + 1)\exp(j\psi_{m,k})}{1 + jQ_{Load,k}\left(\frac{f_i}{f_{o,k}} - \frac{f_{o,k}}{f_i}\right)} - \exp(j\psi_{m,k}) \right\} \right|, \\ ERROR_n &= \frac{1}{I}\sum_{i=1}^{I} \left| S_{n,n}(f_i) - \sum_{k=1}^{K} \left\{ \frac{(\Gamma_{n,k} + 1)\exp(j\psi_{n,k})}{1 + jQ_{Load,k}\left(\frac{f_i}{f_{o,k}} - \frac{f_{o,k}}{f_i}\right)} - \exp(j\psi_{n,k}) \right\} \right| \end{aligned} \tag{5}$$

To find $\Gamma_{m,k}$ and $\exp(j\psi_{m,k})$ we can require $S_{m,m}(f_{i(k)}) = S_{m,m\,app}(f_{i(k)})$ for some K frequencies from the frequency band under investigation. So we can write set of **nonlinear** equations for complex values $X_{m,k} = (\Gamma_{m,k} + 1)\exp(j\psi_{m,k})$ in the following form

$$\sum_{k=1}^{K} \frac{X_{m,k}}{1 + jQ_{Load,k}\left(\frac{f_{i(k)}}{f_{o,k}} - \frac{f_{ok}}{f_{i(k)}}\right)} = S_{m,m}(f_{i(k)}) + \sum_{k=1}^{K} \exp(j\psi_{m,k}) \tag{6}$$

where $\exp(j\psi_{m,k}) = X_{m,k}/|X_{m,k}|$ and we can iterate to find $X_{m,k}$ (in the first iteration we assume $\exp(j\psi_{m,k}) = 1$ and then $\exp(j\psi_{m,k}) = X_{m,k}/|X_{m,k}|$).

Solving these nonlinear equations for $X_{m,k}$ we obtain $\Gamma_{m,k} = |X_{m,k}| - 1$ and can find external Q-factor $Q_{ext\ m,n\ k}$ corresponding to the k-th resonance and ports m and n.

Really

$$\Gamma_{m,k} = \frac{\chi_{m,k} - 1 - \chi_{n,k} - \sum\limits_{\substack{p=1 \\ p\neq m,n}}^{N} \chi_{p,k}}{1 + \sum\limits_{p=1}^{N} \chi_{p,k}}, \quad \Gamma_{n,k} = \frac{\chi_{n,k} - 1 - \chi_{m,k} - \sum\limits_{\substack{p=1 \\ p\neq m,n}}^{N} \chi_{p,k}}{1 + \sum\limits_{p=1}^{N} \chi_{p,k}},$$

$$Q_{Load,k} = \frac{Q_{o,k}}{1 + \sum\limits_{p=1}^{N} \chi_{p,k}}, \tag{7}$$

$$Q_{ext\ m,n\ k} = \frac{Q_{o,k}}{\chi_{m,k} + \chi_{n,k}} = \frac{2Q_{Load,k}}{2 + \Gamma_{m,k} + \Gamma_{n,k}}$$

One can also find the full external Q-factor $Q_{ext,k}$ and $Q_{o,k}$ as follows

$$Q_{ext,k} = \frac{Q_{o,k}}{\sum\limits_{p=1}^{N} \chi_{p,k}} = \frac{2(N-1)}{\sum\limits_{\substack{m,n=1 \\ m\neq n}}^{N} Q^{-1}_{ext\ m,n\ k}}, \quad Q_{o,k} = \frac{Q_{ext,k} Q_{Load,k}}{Q_{ext,k} - Q_{Load,k}} \tag{8}$$

Here $\chi_{p,k}$ represents the coupling factor between p-th port and cavity corresponding to the k-th resonance, $\Gamma_{m,k}$ represents the reflection factor in the reference plane of the m-th port and $\psi_{m,k}$ is defined by the real reference plane position in the m-th port.

We can consider ERROR-functions $ERROR_m$ and $ERROR_n$ as function of only $f_{o,k}$ and $Q_{Load,k}$ (2K unknown parameters). To minimize these ERROR-functions we can use the following procedure. First we change only $f_{o,1}$ and $Q_{Load,1}$ (other $f_{o,k}$ and $Q_{Load,k}$ are fixed). Then we change only $f_{o,2}$ and $Q_{Load,2}$ and so on up to $f_{o,K}$ and $Q_{Load,K}$. This cycle can be repeated many times. After any change in $f_{o,k}$ and/or $Q_{Load,k}$ we have to calculate the complex coefficients $X_{m,k}$ and $X_{n,k}$ using the set of equation (6). So in each step of minimization the ERROR-functions are functions of only two variables.

If we know that the system has resonances outside the frequency band from f_1 to f_I we have to add one or two additional terms in the expressions (4), (5) and (6) corresponding to i = 1 and/or i = I. These additional terms are required to replace resonances located outside the frequency band from f_1 to f_I (lower than f_1 and/or higher than f_I).

Of course we should obtain the same values of $f_{o,k}$ and $Q_{Load,k}$ from the ERROR-functions $ERROR_m$ and $ERROR_n$. So we can use $f_{o,k}$ and $Q_{Load,k}$ obtained from one of the ERROR-functions as initial data for the other one. Using different ERROR-functions produces very small differences in the $f_{o,k}$ and $Q_{Load,k}$ values, due to measurement and numerical errors.

For a 2-port device (N=2, m,n=1,2) expressions (7) and (8) take the form

$$\Gamma_{1,k} = \frac{\chi_{1,k} - 1 - \chi_{2,k}}{1 + \chi_{1,k} + \chi_{2,k}}, \qquad \Gamma_{2,k} = \frac{\chi_{2,k} - 1 - \chi_{1,k}}{1 + \chi_{1,k} + \chi_{2,k}},$$

$$Q_{Load,k} = \frac{Q_{o,k}}{1 + \chi_{1,k} + \chi_{2,k}},$$

$$Q_{ext,k} = \frac{Q_{o,k}}{\chi_{1,k} + \chi_{2,k}} = \frac{2Q_{Load,k}}{2 + \Gamma_{1,k} + \Gamma_{2,k}} \tag{9}$$

$$Q_{o,k} = \frac{Q_{ext,k} Q_{Load,k}}{Q_{ext,k} - Q_{Load,k}}$$

3. Numerical Investigation of Accelerating Modules.

In this section we present examples of calculation carried out for the TTF cavity-coupler unit, for a combination of some cavity-coupler units and for an 8-cavity accelerating module at the frequency band corresponding to the 3rd dipole band of the 9-cell TTF cavity (2470 MHz – 2580 MHz). Each cavity-coupler unit contains only DESY-type HOMCs and DESY-II type FMC. Here we use S-parameters calculated for different sub-units. The detailed description of the S-parameter calculation for different sub-units can be found in [4].

3.1. One Cavity-Coupler Unit.

In this subsection we study the cavity-coupler unit shown in Fig.1. We use complex transmission coefficient $S_{4,1}(f)$ dependence on frequency (transmission between coaxial ports of upstream and downstream HOMCs) to calculate resonance frequencies and Q-factors (left and right beam-pipes are terminated by the matched loads or are infinitely long).

The first resonance curve in Fig.5 shows the absolute value of the complex transmission coefficient $S_{4,1}$ as a function of frequency and second curve shows the complex transmission coefficient $S_{4,1}$ on the complex plane. Solid curve corresponds to initial calculated transmission coefficient $S_{4,1}$ dependence on frequency and (+)-curve was calculated with approximation (1) using ERROR-function minimization.

There are eight resonant frequencies (K = 8) in the frequency band from 2470 MHz to 2582 MHz corresponding to the 3rd dipole mode of the TTF 9-cell cavity. Resonant frequencies and Q-factors also are shown in Fig.5. In this sample we used a frequency step $\Delta f = 2\times10^{-2}$ MHz and obtained ERROR = 3.369×10^{-5}. There are no additional terms because there are no resonant frequencies outside the frequency band from 2470 MHz to 2582 MHz.

One can see very good agreement between the dependence on frequency of the approximating function $S_{4,1\ app}(f)$ and the initial (calculated) transmission coefficient $S_{4,1}$. The maximum distance between initial curve (solid) and approximated curve (+) is equal to 1.149×10^{-4}.

The calculated Q-factors shown in Fig5 are not large due to the very high coupling between cavity and matched left and right beam-pipes (beam-pipe cut off frequency $f_{cut\ H11}$ = 2252.544442 MHz) and there are no trapped modes in the frequency band investigated.

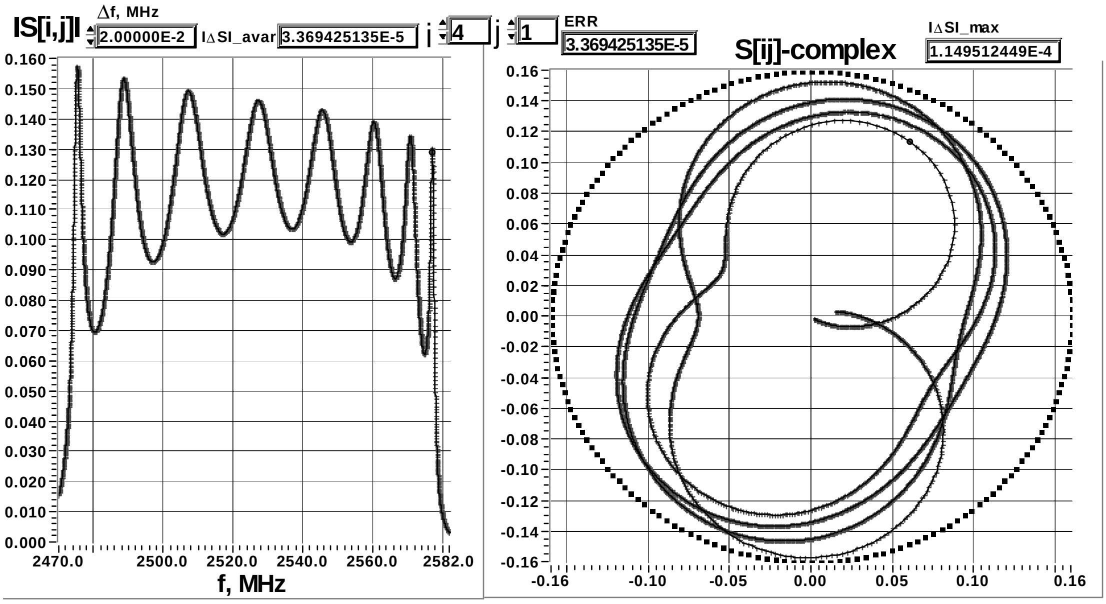

f_res, MHz	Q_res
2475.213749489	1219.7
2488.362997258	387.0
2506.999028541	248.7
2527.271397713	227.6
2545.826206103	265.6
2560.637315171	384.6
2571.058289676	744.0
2577.205428004	2714.8

Fig.5. TTF cavity-coupler unit resonance curves.

3.2. Three Cavity-Coupler Units (no cavity detuning).

In this subsection we study a module consisting of three cavity-coupler units. The cavity-coupler units are connected to each other by cylindrical 78-mm diameter bellows. Matched loads terminate the left beam-pipe of the first cavity-coupler unit and the right beam-pipe of the third cavity-coupler unit. The schematic representation of the 3-cavity module is similar to that shown in Fig.4 and is considered as 6-port system (coaxial ports of upstream and downstream HOMCs, four loads are matched). There is no frequency detuning of the cavities and no other changes in the design of any sub-units.

Resonance curves of the system consisting of three cavity-coupler units are shown in Fig.6. The investigation was carried out in the frequency range from 2575 MHz to 2582 MHz with a frequency step of $\Delta f = 5\times10^{-3}$ MHz.

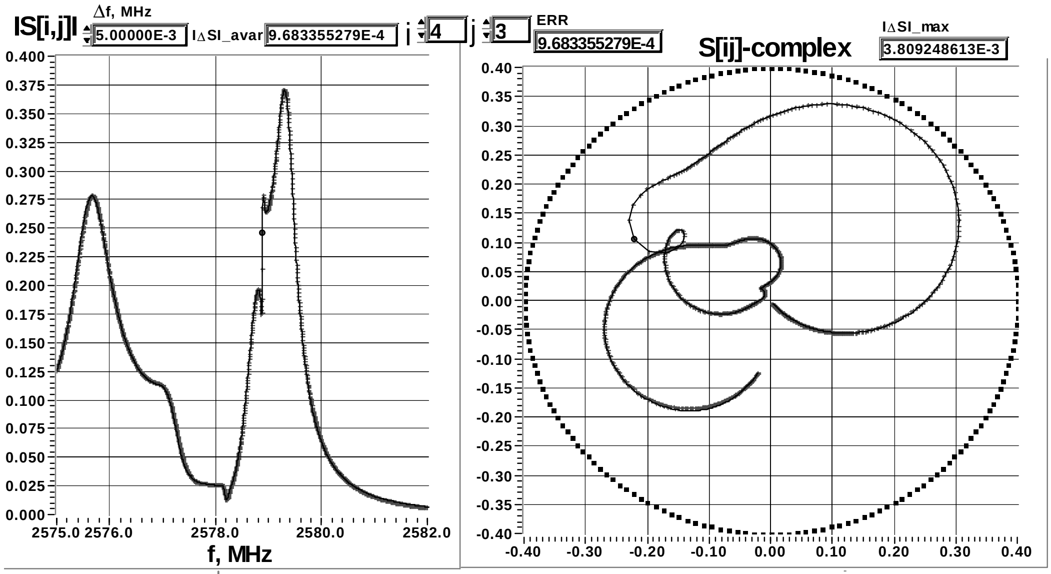

f_res, MHz	Q_res
2575.652897344	3720.6
2577.174718251	4746.0
2578.187620867	19816.0
2578.703114546	5567.4
2578.882760001	84678.1
2579.336170880	6756.3
2573.009854968	6049150.6

Fig.6. Three cavity module resonance curves (no cavity detuning).

We used transmission coefficient $S_{4,5}(f)$ dependence on frequency (coaxial ports of the upstream and downstream HOMCs of the second cavity-coupler unit) to calculate the resonant frequencies and Q-factors. Here we found six resonances in the investigated frequency band and used one additional term with the resonant frequency below the frequency band under investigation. This additional term replaces all other resonances located bellow the frequency band investigated. One can see good agreement between the initial (solid) and approximated (+) resonance curves ($ERROR_{av} = 0.96834\times10^{-3}$, $ERROR_{max} = 3.809\times10^{-3}$).

There are two resonances with a relatively high Q-factor: f_{res} = 2578.882760MHz, Q = 84678 and f_{res} = 2578.187621 MHz, Q = 19816. Other resonances have lower Q-factor values.

3.3. Three Cavity-Coupler Units (+10 MHz detuning of 2^{nd} cavity).

In this subsection we study a module consisting of three cavity-coupler units. This module differs from the preceding one in +10 MHz frequency detuning of the second cavity. Resonance curves of this system are shown in Fig.7. The investigation was carried out in the frequency band from 2569 MHz up to 2589 MHz with frequency step $\Delta f = 4\times10^{-3}$ MHz. We used transmission coefficient $S_{4,3}(f)$ dependence on frequency (coaxial ports of the upstream and downstream HOMCs of the second cavity-coupler unit) to calculate the resonant frequencies and Q-factors.

Here we found ten resonances in the frequency band investigated and used one additional term with the resonance frequency below that frequency band. One can see good agreement between the initial (solid) and approximated (+) resonance curves ($ERROR_{av} = 5.977\times10^{-4}$, $ERROR_{max} = 6.460\times10^{-3}$) and three resonances with very high Q-factor: f_{res} = 2587.740251 MHz, Q = 1005536; f_{res} = 2583.470705 MHz, Q = 320271; f_{res} = 2578.712716 MHz, Q = 46101. The highest three modes look like double resonances corresponding to a double polarization of each mode. Both HOMCs of the second cavity-coupler unit have very weak coupling to the field of one polarization and strong coupling to the field of the other. The matched loads terminating the left beam-pipe of the first cavity-coupler unit and the right beam-pipe of the third cavity-coupler unit cannot provide strong suppression of these modes due to the large detuning of the second cavity.

The frequency dependence of the complex transmission coefficient plotted on the complex plane shows that only few points are located on the resonance curve, corresponding to high Q-factor resonances (Q = 1005536 and Q = 320271). These two resonance curves are shown in Fig.7 as straight lines. This is because we used a large frequency step $\Delta f = 4\times10^{-3}$ MHz in our calculation. The resonance of the 3 dB band is equal to 2.587×10^{-3} MHz for $Q = 10^{+6}$. So we used a frequency step greater than the resonance of the 3 dB band.

Other resonances have lower values of Q-factor and curves, which correspond to resonances with lower Q-factor, look like circular arcs in Fig.7.

3.4. Eight Cavity-Coupler Units (no cavity detuning).

In this subsection we study a module consisting of eight cavity-coupler units. The cavity-coupler units are connected to each other by cylindrical 78-mm diameter bellows. Matched loads terminate the left beam-pipe of the first cavity-coupler unit and the right beam-pipe of the eighth cavity-coupler unit. A schematic representation of the 8-cavity module is shown in Fig.4 and the 8-cavity module is considered as a 16-port system (coaxial ports of upstream and downstream HOMCs, four loads are matched). There is no frequency detuning of the cavities and no other changes in the design of any sub-unit.

Resonance curves of the system consisting of eight cavity-coupler units are shown in Fig.8. The investigation was carried out in the frequency band from 2578 MHz to 2580 MHz (only 2 MHz frequency band) with frequency step $\Delta f = 2\times10^{-3}$ MHz.

We used the dependence of the transmission coefficient $S_{10,9}(f)$ on frequency (coaxial ports of the upstream and downstream HOMCs of the fifth cavity-coupler unit) to calculate the resonant frequencies and Q-factors. One can see good agreement between initial (solid) and approximated (+) resonance curves ($ERROR_{av} = 1.977\times10^{-4}$, $ERROR_{max} = 7.773\times10^{-4}$).

D_DD2 (0 MHz), D_DD2 (+10 MHz), D_DD2 (0 MHz)

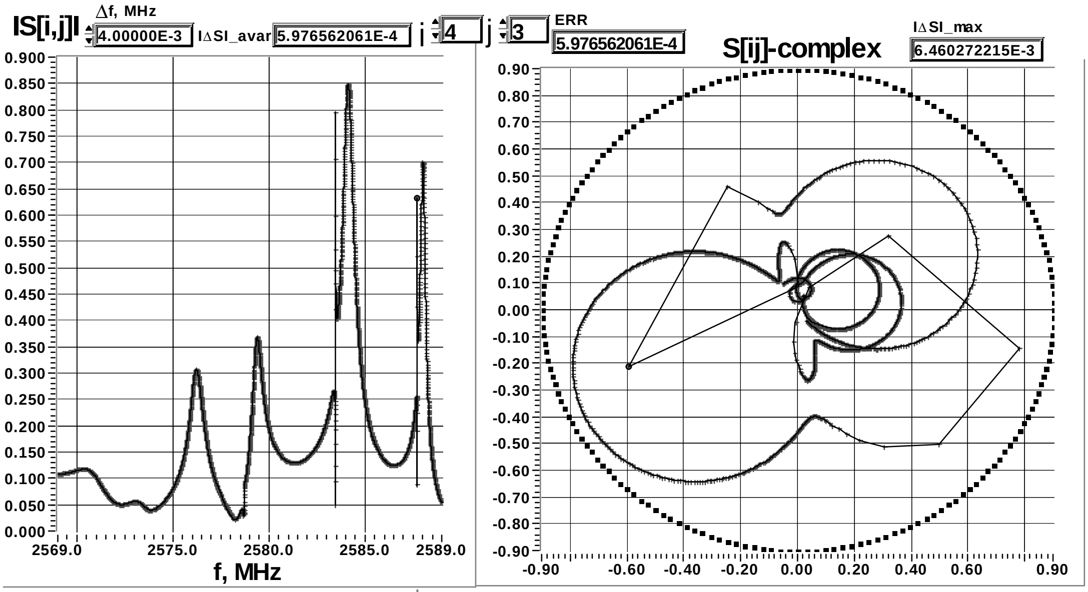

f_res, MHz	Q_res
2570.866511222	1301.5
2573.296488717	2177.5
2576.115295021	1866.8
2576.212630159	3697.5
2578.712715736	46101.1
2579.336612254	5085.9
2583.470704806	320271.2
2584.129609289	4880.2
2587.740251372	1005536.0
2588.024246357	10995.6
2566.147775371	1420.6

Fig.7. Three-cavity module resonance curves (+10 MHz second cavity detuning)

D_DD2(0 MHz), D_DD2(0 MHz), D_DD2(0 MHz), D_DD2(0 MHz), D_DD2(0 MHz), D_DD2(0 MHz), D_DD2(0 MHz), D_DD2(0 MHz)

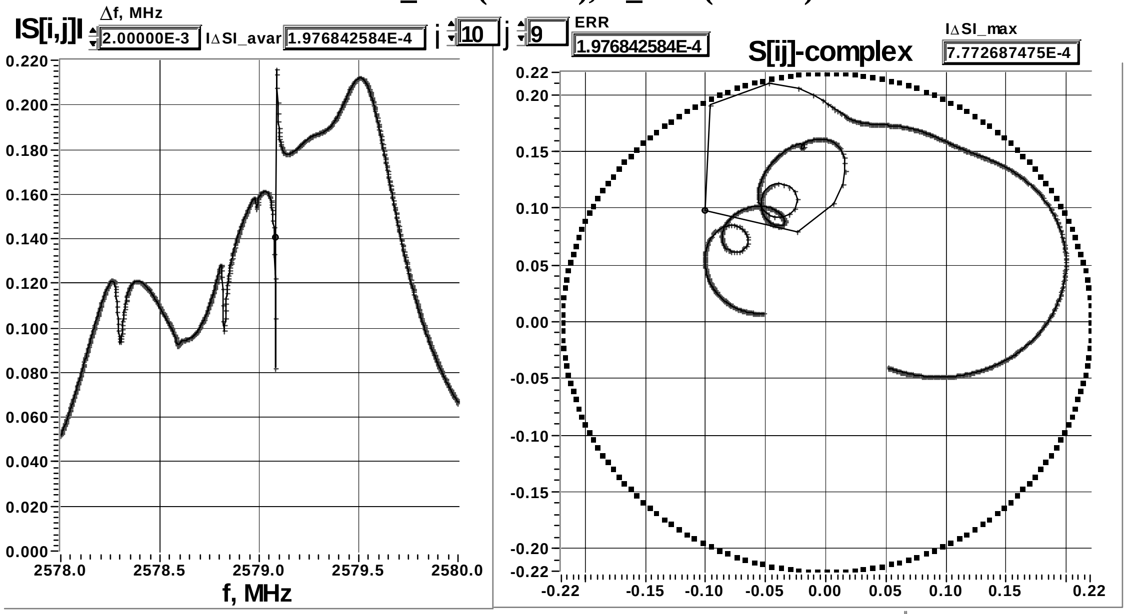

f_res, MHz	Q_res
2579.522376042	7209.1
2579.261796493	5768.7
2579.084344026	540112.6
2579.106327605	6537.9
2578.947422951	7981.0
2578.819221893	158993.8
2578.224729691	4353.4
2578.326819946	4237.9
2578.293757759	63438.8
2578.698898996	4043.4
2577.006013979	5690.9
2578.985193016	282315.7
2578.592676231	86270.8

Fig.8. Eight-cavity module resonance curves. (no cavity detuning)

There are a lot of resonances in the narrow frequency band (2 MHz) and three resonances with relatively high Q-factor: f_{res} = 2579.084344 MHz, Q = 540112; f_{res} = 2578.985193 MHz, Q = 282316; f_{res} = 2578.819222 MHz, Q = 158994. Other resonances have a lower Q-factor.

3.5. Eight Cavity-Coupler Units (+10 MHz detuning of 4th cavity).

In this subsection we study a module consisting of eight cavity-coupler units. This module differs from the preceding one in +10 MHz frequency detuning of the fourth cavity. Resonance curves of this system are shown in Fig.9. The investigation was carried out in the frequency range from 2582 MHz to 2589 MHz with frequency step $\Delta f = 4\times10^{-3}$ MHz. We used the dependence of the transmission coefficient $S_{8,7}(f)$ on frequency (coaxial ports of the upstream and downstream HOMCs of the fourth cavity-coupler unit) to calculate resonant frequencies and Q-factors.

One can see good agreement between the initial (solid) and approximated (+) resonance curves ($ERROR_{av} = 5.665\times10^{-5}$, $ERROR_{max} = 4.294\times10^{-4}$). One can see two resonances with a very high Q-factor: f_{res} = 2587.740254 MHz, Q = 1006630; f_{res} = 2583.470976 MHz, Q = 329389 **(compare Fig.7, subsection 3.3)**. Here two modes look like double resonances corresponding to double polarization of each mode. Both HOMCs of the fourth cavity-coupler unit have very weak coupling with field of one polarization and strong coupling with field of other polarization. The matched loads terminating the left beam-pipe of the first cavity-coupler unit and the right beam-pipe of the eighth cavity-coupler unit cannot provide strong suppression of these modes due to the large detuning of the fourth cavity.

Frequency dependence of the complex transmission coefficient plotted on the complex plane shows that only few points are located on the resonance curve corresponding to high Q-factor resonance (Q = 1006630 and Q = 329389). These two resonance curves are shown in Fig.9 as straight lines. This has the same reason as in Section 3.3. Other resonances have lower values of Q-factor and curves, which correspond to resonances with lower Q-factor, looks like circular arcs in Fig.9.

3.6. Eight Cavity-Coupler Units Module with Short Circuited Beam Pipes.

In this subsection we study a module consisting of eight cavity-coupler units. There is no frequency detuning of the cavities and no other changes in design of any sub-units. The cavity-coupler units are connected to each other by cylindrical 78-mm diameter bellows. Left beam-pipe of the first cavity-coupler unit and right beam-pipe of the eighth cavity-coupler unit are terminated by short circuiting loads at the 0.01m distance from the corresponding reference planes. A schematic representation of the 8-cavity module is shown in Fig.4 and 8-cavity module is considered as a 16-port system (coaxial ports of upstream and downstream HOMCs).

Resonance curves of this system are shown in Fig.10. The investigation was carried out in the frequency band from 2572 MHz to 2576 MHz (there are some resonances below 2572 MHz and higher than 2576 MHz) with a frequency step $\Delta f = 2\times10^{-3}$ MHz. We used the dependence of the transmission coefficient $S_{10,9}(f)$ on frequency (coaxial ports of the upstream and downstream HOMCs of the fifth cavity-coupler unit) to calculate the resonance frequencies and Q-factors.

D_DD2(0 MHz), D_DD2(0 MHz), D_DD2(0 MHz), D_DD2(+10 MHz), D_DD2(0 MHz), D_DD2(0 MHz), D_DD2(0 MHz), D_DD2(0 MHz)

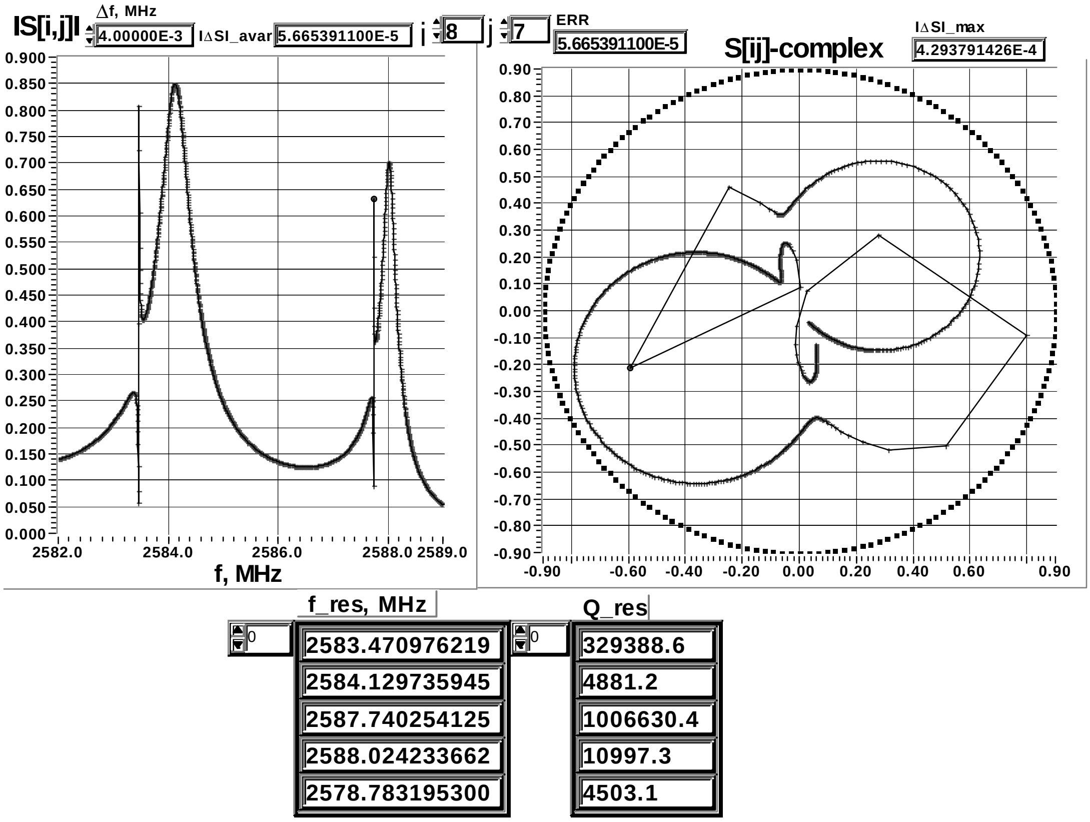

Fig.9. Eight-cavity module resonance curves (+10 MHz fourth cavity detuning)

Figures 10-13 show resonance curves for $S_{10,9}$, $S_{16,1}$, $S_{2,1}$ and $S_{8,7}$ respectively.

ACCELERATING MODULE of 8 cavity-coupler units:
(0) D_DD2 (0 MHz), shorted (0.01 m)
(1) D_DD2 (0 MHz), (2) D_DD2 (0 MHz),
(3) D_DD2 (0 MHz), (4) D_DD2 (0 MHz),
(5) D_DD2 (0 MHz), (6) D_DD2 (0 MHz),
(7) D_DD2 (0 MHz), shorted (0.01 m).

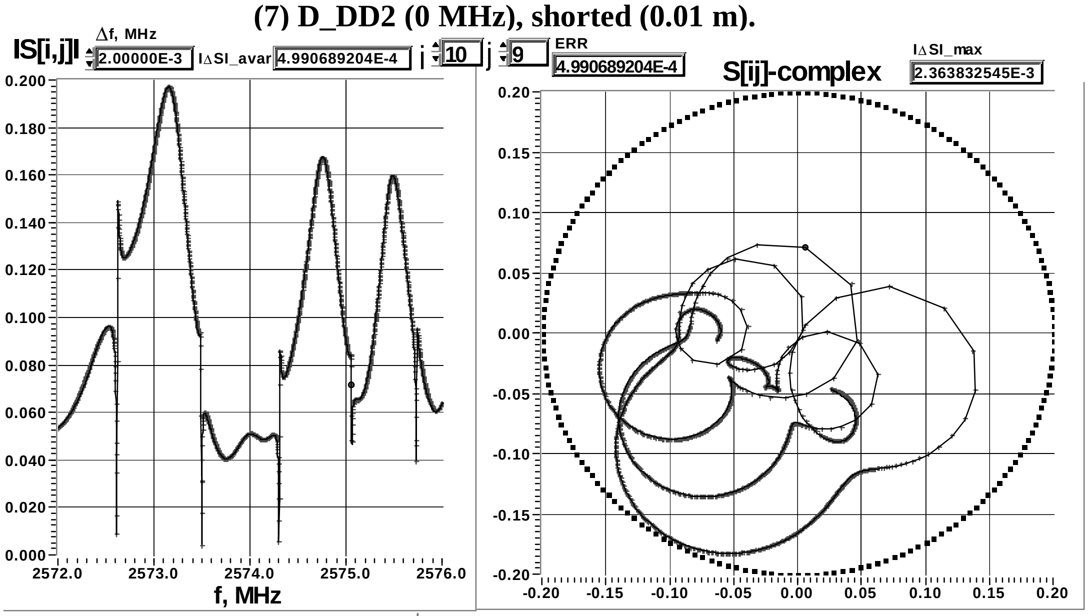

f_res, MHz	Q_res
2572.616903243	208873.7
2572.386619577	3800.3
2573.200122579	6128.5
2573.492770103	234861.8
2573.840892673	5104.8
2574.034412096	7501.6
2574.308683706	249278.5
2574.773545869	7172.7
2575.057962314	254896.1
2575.474487203	7899.6
2575.735016805	260563.4
2576.156008290	4924.4
2571.065395734	7039110.2

Fig.10. Eight-cavity module resonance $S_{10,9}$ (f) curves.
Left and right beam-pipes are short circuited.

Here one can find eleven resonances in the frequency band of 4 MHz bandwidth and two additional terms to replace other resonances (lower and upper investigated frequency band). There are four resonances with high Q-factor: f_{res} = 2572.616903 MHz, Q = 208873; f_{res} = 2573.492770 MHz, Q = 234862; f_{res} = 2574.308683 MHz, Q = 249279; f_{res} = 2575.735502 MHz, Q = 260563. One can see good agreement between the initial (solid) and approximated (+) resonance curves ($ERROR_{av}$ = 4.991×10^{-4}, $ERROR_{max}$ = 2.364×10^{-3}).

The next figure (Fig.11) shows resonance curves for the same 8-cavity module calculated with $S_{16,1}(f)$ dependence on frequency.

ACCELERATING MODULE of 8 cavity-coupler units:
(0) D_DD2 (0 MHz), shorted (0.01 m); (1) D_DD2 (0 MHz),
(2) D_DD2 (0 MHz), (3) D_DD2 (0 MHz), (4) D_DD2 (0 MHz),
(5) D_DD2 (0 MHz), (6) D_DD2 (0 MHz),
(7) D_DD2 (0 MHz), shorted (0.01 m)

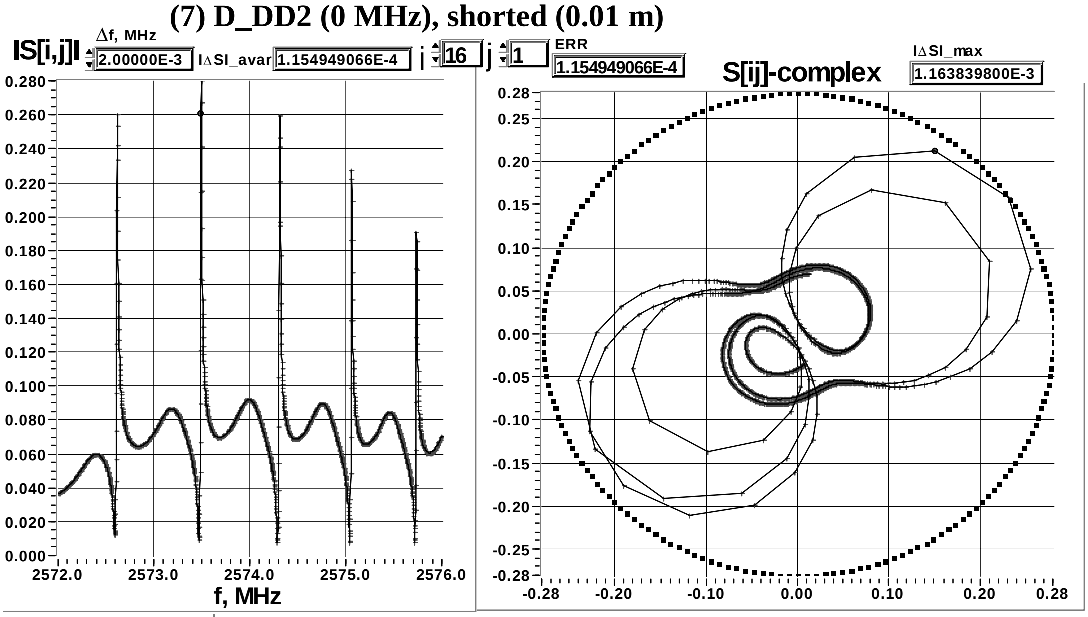

f_res, MHz	Q_res
2572.407815650	5434.2
2572.616946852	209285.8
2573.202608767	6028.6
2573.492787969	236435.3
2574.010379223	6569.5
2574.308722812	248210.0
2574.774442064	7207.6
2575.057931879	254981.5
2575.476771331	7819.2
2575.735048194	259178.2
2576.084060933	11468.8
2571.566833801	10811.7

Fig.11. Eight-cavity module resonance $S_{16,1}(f)$ curves
Left and right beam-pipes are shorted

Here there are ten resonances in the frequency band. There are five resonances with high Q-factors and five resonances with low Q-factors. $ERROR_{av} = 1.155\times10^{-4}$, $ERROR_{max} = 1.163\times10^{-3}$.

Fig. 12 shows resonance curves for the same 8-cavity module calculated with $S_{2,1}(f)$ dependence on frequency. $ERROR_{av} = 8.988\times10^{-4}$, $ERROR_{max} = 3.904\times10^{-3}$. Here one can find ten resonances in the frequency band of 4 MHz bandwidth and two additional terms to replace other resonances (lower and upper investigated frequency band). There are five resonances with high Q-factors and five resonances with low Q-factors shown in Fig.12.

ACCELERATING MODULE of 8 cavity-coupler units:
(0) D_DD2 (0 MHz), shorted (0.01 m); (1) D_DD2 (0 MHz),
(2) D_DD2 (0 MHz), (3) D_DD2 (0 MHz), (4) D_DD2 (0 MHz),
(5) D_DD2 (0 MHz), (6) D_DD2 (0 MHz),
(7) D_DD2 (0 MHz), shorted (0.01 m).

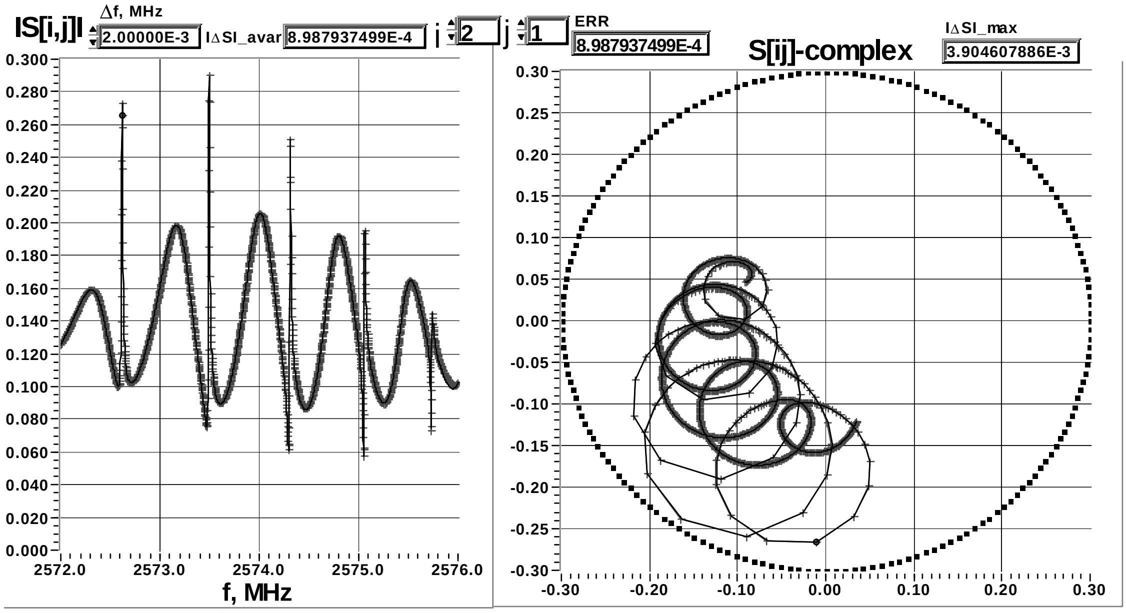

	f_res, MHz		Q_res
0	2572.401961257	0	5802.5
	2572.617004175		211394.9
	2573.204158945		6200.6
	2573.492813357		238491.8
	2574.011915083		6682.7
	2574.308739940		249980.4
	2574.775517346		7327.3
	2575.057932149		257243.7
	2575.476615645		8450.7
	2575.734840381		275791.4
	2570.380427608		2409403.7
	2576.133256692		718829.6

Fig.12. Eight-cavity module resonance $S_{2,1}(f)$ curves
Left and right beam-pipes are shorted

ACCELERATING MODULE of 8 cavity-coupler units:

(0) D_DD2 (0 MHz), shorted (0.01 m); (1) D_DD2 (0 MHz),
(2) D_DD2 (0 MHz), (3) D_DD2 (0 MHz), (4) D_DD2 (0 MHz),
(5) D_DD2 (0 MHz), (6) D_DD2 (0 MHz),
(7) D_DD2 (0 MHz), shorted (0.01 m).

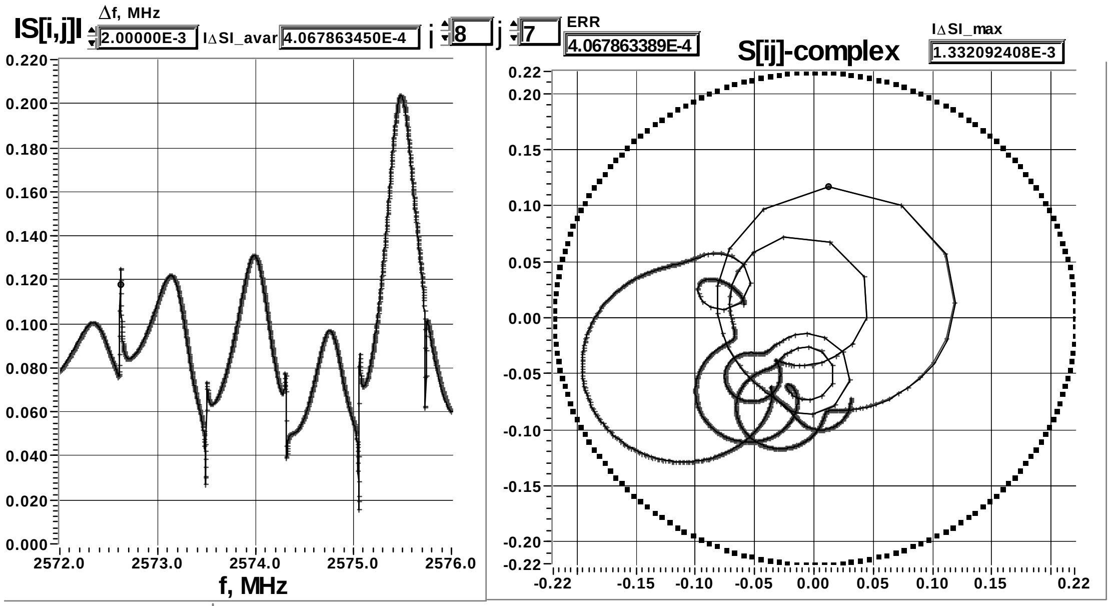

f_res, MHz	Q_res
2572.616902053	209168.8
2573.203904954	6191.4
2573.492707180	239591.6
2574.010399374	6615.5
2574.308714094	247916.7
2574.772722926	7245.0
2575.057925026	252305.1
2575.475162060	7993.4
2575.734898945	257920.3
2576.306703212	6386.0
2569.217667094	329931898(
2572.395137515	5926.0

Fig.13. Eight-cavity module resonance $S_{8,7}(f)$ curves
Left and right beam-pipes are shorted

Fig. 13 shows resonance curves for the same 8-cavity module calculated with $S_{8,7}(f)$ dependence on frequency. $ERROR_{av} = 4.068\times10^{-4}$, $ERROR_{max} = 1.332\times10^{-3}$. Here there are ten resonances in the frequency band. Figure 13 shows five resonances with high Q-factors and five resonances with low Q-factors.

Let us compare the results represented in Fig.10, 11, 12 and 13. These data were obtained with different transmission coefficients and the resonance curves look very different. However the resonant frequencies and Q-factors calculated with these transmission coefficient dependencies on frequency are very close to each other. The following table illustrates this.

	Fig.10	Fig.11	Fig.12	Fig.13
f_{res}, MHz Q	2572.387 3800	2572.408 5430	2572.402 5802	2572.395 5930
f_{res}, MHz Q	2572.617 208870	2572.617 209290	2572.617 211390	2572.617 209170
f_{res}, MHz Q	2573.200 6130	2573.203 6030	2573.204 6200	2573.204 6190
f_{res}, MHz Q	2573.493 234860	2573.493 236440	2573.493 238490	2573.493 239590
f_{res}, MHz Q	2574.034 7500	2574.010 6570	2574.012 6680	2574.010 6620
f_{res}, MHz Q	2574.309 249280	2574.309 248210	2574.309 249980	2574.309 247920
f_{res}, MHz Q	2574.774 7170	2574.774 7210	2574.776 7330	2574.773 7250
f_{res}, MHz Q	2575.058 254900	2575.058 254980	2575.058 257240	2575.058 252310
f_{res}, MHz Q	2575.474 7900	2575.477 7820	2575.477 84590	2575.475 7990
f_{res}, MHz Q	2575.735 260560	2575.735 259180	2575.745 275790	2575.735 257920

3.7. Two Cavity-Coupler Units Module with Short Circuited Beam Pipes.

In this subsection we study a module consisting of two cavity-coupler units. There is no frequency detuning of the cavities and no other changes in design of any sub-units. The cavity-coupler units are connected to each other by cylindrical 78-mm diameter bellows. The left beam-pipe of the first cavity-coupler unit and the right beam-pipe of the second cavity-coupler unit are terminated by short circuiting loads at 0.1m distance from the corresponding reference planes. The schematic representation of the 2-cavity module is similar to the module shown in Fig.4 and the 2-cavity module is considered as a 4-port system (coaxial ports of upstream and downstream HOMCs).

ACCELERATING MODULE of two cavity-coupler units:
(0) D_DD2 (0 MHz), shorted (0.1 m); (1) D_DD2 (0 MHz), shorted (0.1 m).

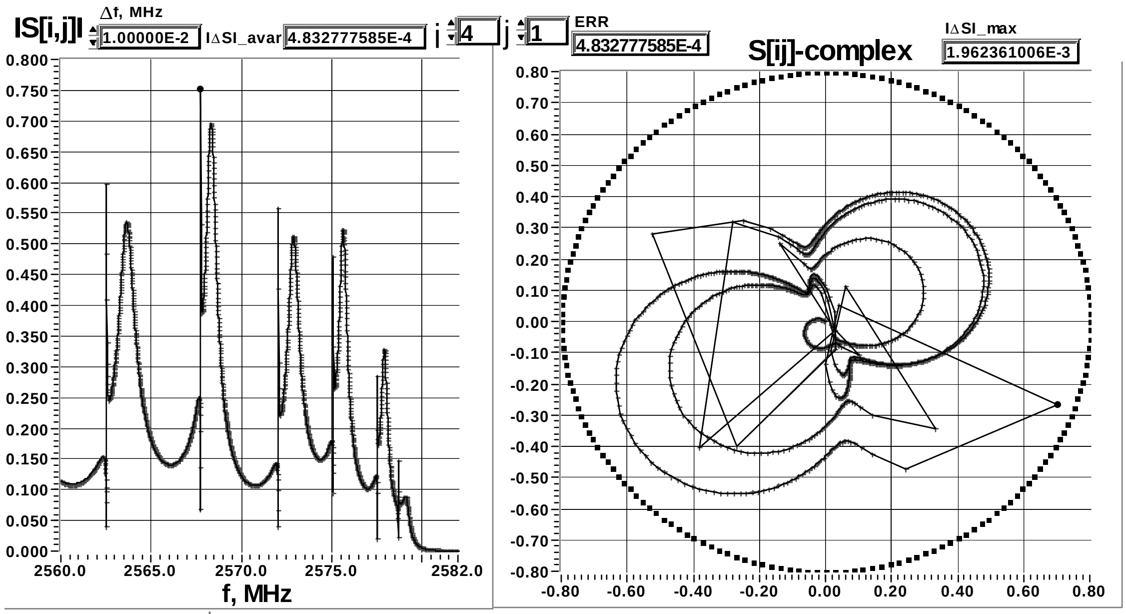

f_res, MHz	Q_res
2562.543470766	223234.1
2563.649081253	3045.8
2567.757727663	293177.5
2568.332739822	4733.8
2572.061518486	367656.1
2572.889378324	4417.5
2575.104813482	408321.7
2575.652730792	6149.1
2577.534791511	1306532.1
2577.936262635	8148.8
2578.706003895	827858.4
2579.163486409	7127.3
2558.119745971	6837.9

Fig.14. Two-cavity module resonance $S_{4,1}(f)$ curves
Left and right beam-pipes are shorted

Resonance curves of this system are shown in Fig.14. The investigation was carried out in the frequency band from 2560 MHz to 2582 MHz (22 MHz frequency band, there are some resonances below 2560 MHz) with frequency step $\Delta f = 10^{-2}$ MHz. We used transmission coefficient $S_{4,1}(f)$ dependence on frequency (coaxial ports of the first upstream and last downstream HOMCs) to calculate the resonant frequencies and Q-factors. There are twelve resonances in the frequency band from 2560 MHz to 2582 MHz and one additional term lower 2560 MHz to replace other resonances. $ERROR_{av} = 4.833\times10^{-4}$ and $ERROR_{max} = 1.962\times10^{-3}$.

4. Experimental Investigation of One Cavity-Coupler Unit

In this subsection we present the results of the experimental investigation of one cavity-coupler unit consisting of a copper 9-cell TTF cavity and two (upstream and downstream) DESY-type HOMCs.

The purpose of this investigation is to check our proposal to improve the original HOMC and provide conditions for damping modes in the frequency range of the 3rd dipole band. This proposal consists in "mirror" modification of upstream HOMC as shown in Fig.15.

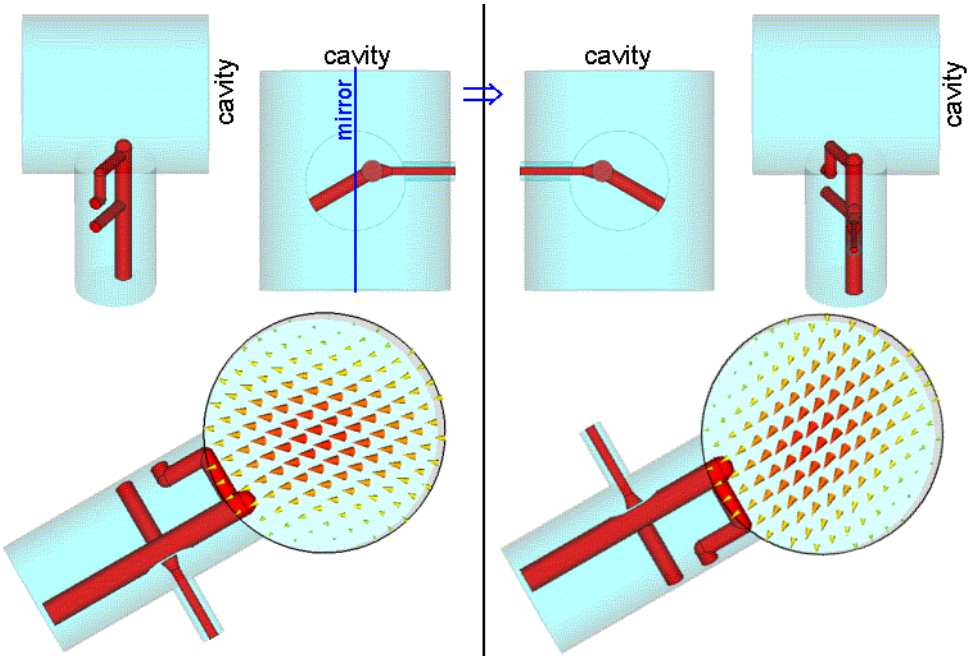

Fig.15 Proposed modification of the downstream HOMC. Due to a 'mirror' transformation the polarisation of maximal coupling is rotated.

Detailed numerical investigation of accelerating modules with modified upstream HOMCs were carried out in work [4]. However to simplify the construction process it is necessary to modify the downstream HOMCs. Numerical investigation of accelerating modules with modified downstream HOMCs was carried out in [5].

Here we carried out an experimental investigation of a TESLA 9-cell copper cavity equipped with two HOMCs (upstream and downstream) and short-circuited beam pipes as shown in Fig.16. The positions of the short circuiting planes were chosen in a such way to provide strong coupling between the HOMCs and the cavity in the frequency range of the 3rd dipole band (the beam pipe cutoff frequency is below the 3rd dipole band). There is no fundamental mode coupler in our experimental set-up. We investigated a cavity-coupler unit equipped with original upstream and downstream HOMCs and with original upstream HOMC and modified ("mirrored") downstream HOMC in the frequency range corresponding to the 1st, 2nd and 3rd dipole band, 2nd monopole band and 2nd quadrupole band.

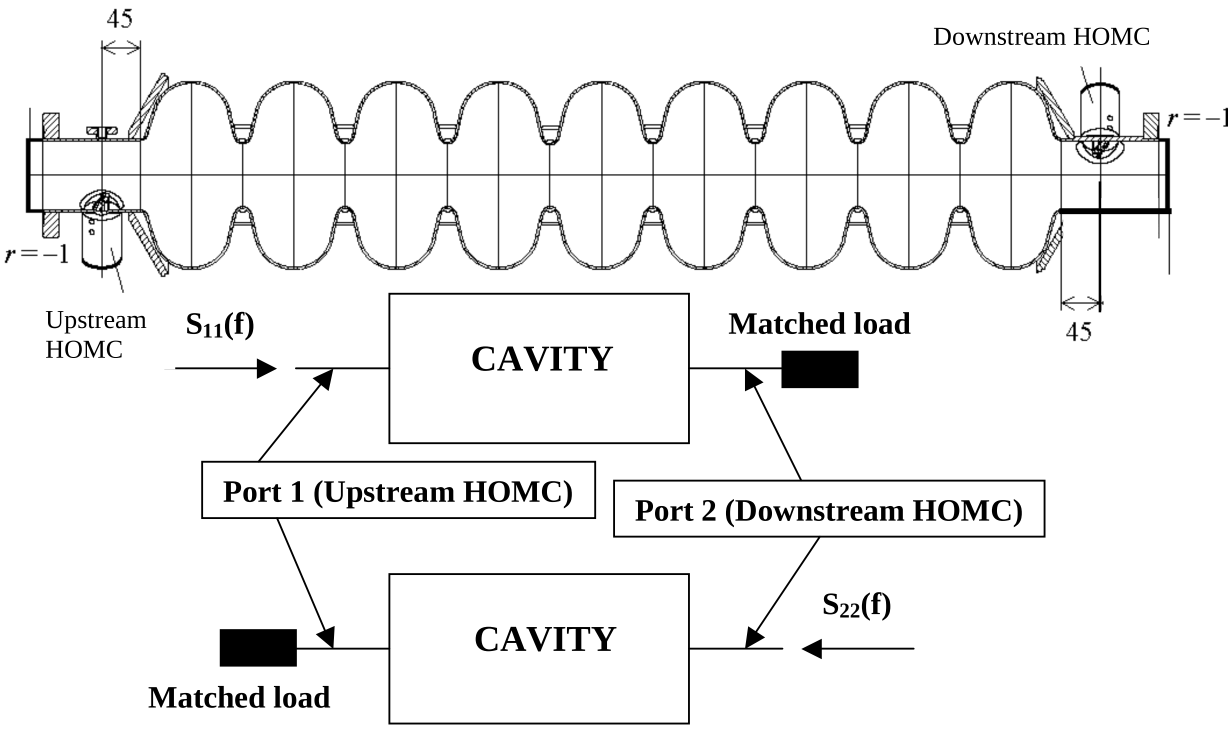

Fig.16 Schematic representation of the experimental set-up

We have here a 2-port device and measure only the reflection coefficients $S_{11}(f)$ and $S_{22}(f)$ as a function of frequency. Measurements of $S_{11}(f)$ and $S_{22}(f)$ with a HP Network Analyzer (NWA) must be carried out in the same frequency band and with the same frequency step ($f_i \Rightarrow f_1, f_2,\ldots, f_i, \ldots, f_I$; $i = 1, 2, 3, \ldots, I$; $\Delta f=f_i - f_{i-1}$). To calculate the resonant frequencies and Q-factors ($Q_{Load,k}$, $Q_{o,k}$, $Q_{ext,k}$) we use a procedure described in section 2. Namely, we minimize two error functions

$$\mathrm{ERROR}_1=\frac{1}{I}\sum_{i=1}^{I}\left|S_{1,1}(f_i)-\sum_{k=1}^{K}\left\{\frac{(\Gamma_{1,k}+1)\exp(j\psi_{1,k})}{1+jQ_{Load,k}\left(\frac{f_i}{f_{o,k}}-\frac{f_{o,k}}{f_i}\right)}-\exp(j\psi_{1,k})\right\}\right|,$$

$$\mathrm{ERROR}_2=\frac{1}{I}\sum_{i=1}^{I}\left|S_{2,2}(f_i)-\sum_{k=1}^{K}\left\{\frac{(\Gamma_{2,k}+1)\exp(j\psi_{2,k})}{1+jQ_{Load,k}\left(\frac{f_i}{f_{o,k}}-\frac{f_{o,k}}{f_i}\right)}-\exp(j\psi_{2,k})\right\}\right| \qquad (5')$$

and solve a set of nonlinear equations at each step of the minimization

$$\sum_{k=1}^{K}\frac{X_{m,k}}{1+jQ_{Load,k}\left(\frac{f_{i(k)}}{f_{o,k}}-\frac{f_{ok}}{f_{i(k)}}\right)}=S_{m,m}(f_{i(k)})+\sum_{k=1}^{K}\exp(j\psi_{m,k}) \qquad (6')$$

where $m = 1, 2$; $\exp(j\psi_{m,k}) = X_{m,k}/|X_{m,k}|$; $\Gamma_{m,k} = |X_{m,k}| - 1$

Then we calculate external the Q-factor $Q_{ext,k}$ and $Q_{o,k}$

$$Q_{ext,k}=\frac{2Q_{Load,k}}{2+\Gamma_{1,k}+\Gamma_{2,k}}$$

$$Q_{o,k}=\frac{Q_{ext,k}Q_{Load,k}}{Q_{ext,k}-Q_{Load,k}} \qquad (9')$$

It is very useful to choose i(1)=1, i(K)=I and to fix $f_{o,1}= f_{i(1)}=f_1$, $Q_{Load,1}=0.1 \ldots 10$ and $f_{oK}= f_{i(K)}=f_I$, $Q_{Load,K}=0.1 \ldots 10$. So the error-function ERROR_m is a function of 2K-2 variables, but a set of equations (6') contains K complex unknown values $X_{m,k}$.

Both error-functions ERROR_1 and ERROR_2 must give us very close resonant frequencies and loaded Q-factors ($f_{o,k}$ and $Q_{Load,k}$). This fact can be used to estimate measurement and calculation errors.

We carried out measurements in the following frequency ranges:

$$\left.\begin{cases} 1622\,\text{MHz} --- 1667\,\text{MHz}\ \ (4\,\text{modes}) \\ 1681\,\text{MHz} --- 1734\,\text{MHz}\ \ (3\,\text{modes}) \\ 1760\,\text{MHz} --- 1803\,\text{MHz}\ \ (3\,\text{modes}) \end{cases}\right\} 1^{st}\ \text{dipole band}\ (10\ \text{double resonances})$$

$$\left.\begin{cases} 1836\,\text{MHz} --- 1889\,\text{MHz} \\ \end{cases}\right\} 2^{nd}\ \text{dipole band (8 double resonances)}$$

$$\left.\begin{cases} 2381\,\text{MHz} --- 2458\,\text{MHz} \\ \end{cases}\right\} 2^{nd}\ \text{monopole band (9 resonances)}$$

$$\left.\begin{cases} 2469\,\text{MHz} --- 2507\,\text{MHz} \\ 2507\,\text{MHz} --- 2582\,\text{MHz}\ \ (6\,\text{modes}) \end{cases}\right\} \begin{cases} 2^{nd}\ \text{quadrupole and} \\ 3^{rd}\ \text{dipole band (8 double resonances)} \end{cases}$$

The most important modes with large (R/Q)-ratio are:

6^{th} and 7^{th} modes of the 1^{st} dipole band;

3^{rd}, 4^{th} and 5^{th} modes of the 2^{nd} dipole band;

8^{th} mode of the 3^{rd} dipole band;

7^{th}, 8^{th} and 9^{th} modes of the 2^{nd} monopole band;

Measurements were carried out with two cavities and for six cavity rotation angles around the cavity axis (0, 30, 60, 90, 120 and 150 degrees; HOMCs position is fixed). There are 1601 points in each frequency range provided by the NWA.

4.1 Practical Examples

Let us consider some practical examples of determination of resonant frequencies and Q-factors.

Fig.17 shows the S_{11} and S_{22} dependence on frequency for a cavity with two original HOMCs. To calculate the resonant frequencies and loaded Q-factors we have used a very narrow frequency range containing only 50 (of 1601) measured points. There are two resonances that correspond to the double polarization of the dipole mode. Resonant frequencies, loaded Q-factors, Γ–values and error-function values are shown in Fig.17 too (f_o=1624.290/1624.288 and 1624.488/1624.488 MHz, Q_{Load}=17510/18510 and 16090/16090). One can see that port 1 has weak coupling with the cavity at the lower resonant frequency and stronger coupling at the higher resonant frequency ($\Gamma = -0.983$ and -0.737 correspondingly). At the same time port 2 has very weak coupling at the higher resonance frequency ($\Gamma = -0.9993$).

Fig.18 shows the same dependencies and values for the cavity with original and modified HOMCs. There are also two resonances that correspond to the double polarization of the dipole mode, but both ports have relatively strong coupling with the cavity. Resonant frequencies, loaded Q-factors, Γ–values and error-function values are also shown in Fig.18 (f_o=1624.289/1624.290 and 1624.483/1624.485 MHz, Q_{Load}=17460/17860 and 15860/15540). One can see good agreement between measured (solid) and approximated (+) resonance curves.

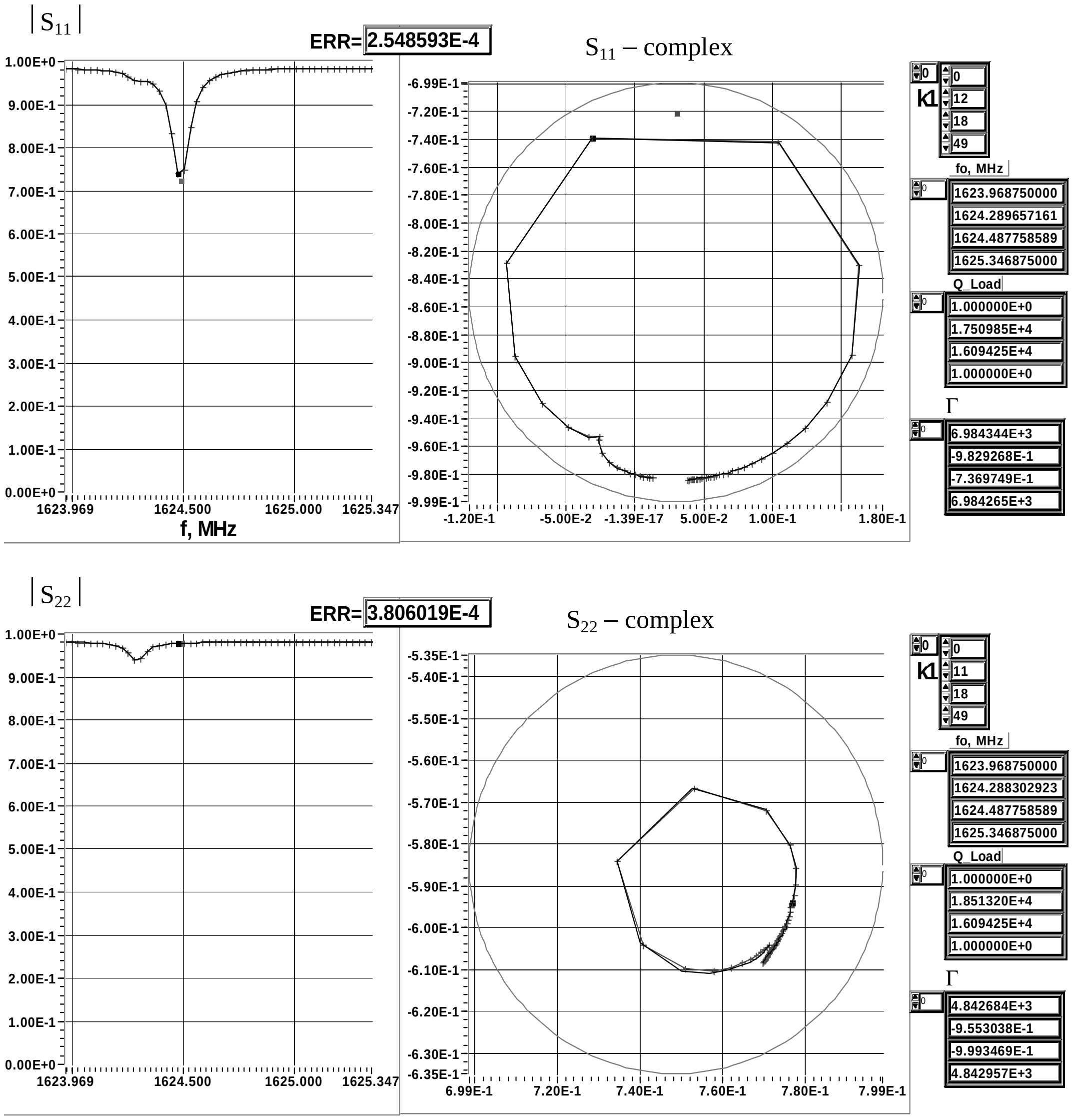

Fig.17 S_{11} and S_{22} dependence on frequency. First dipole band, first mode. Original–original HOMCs.

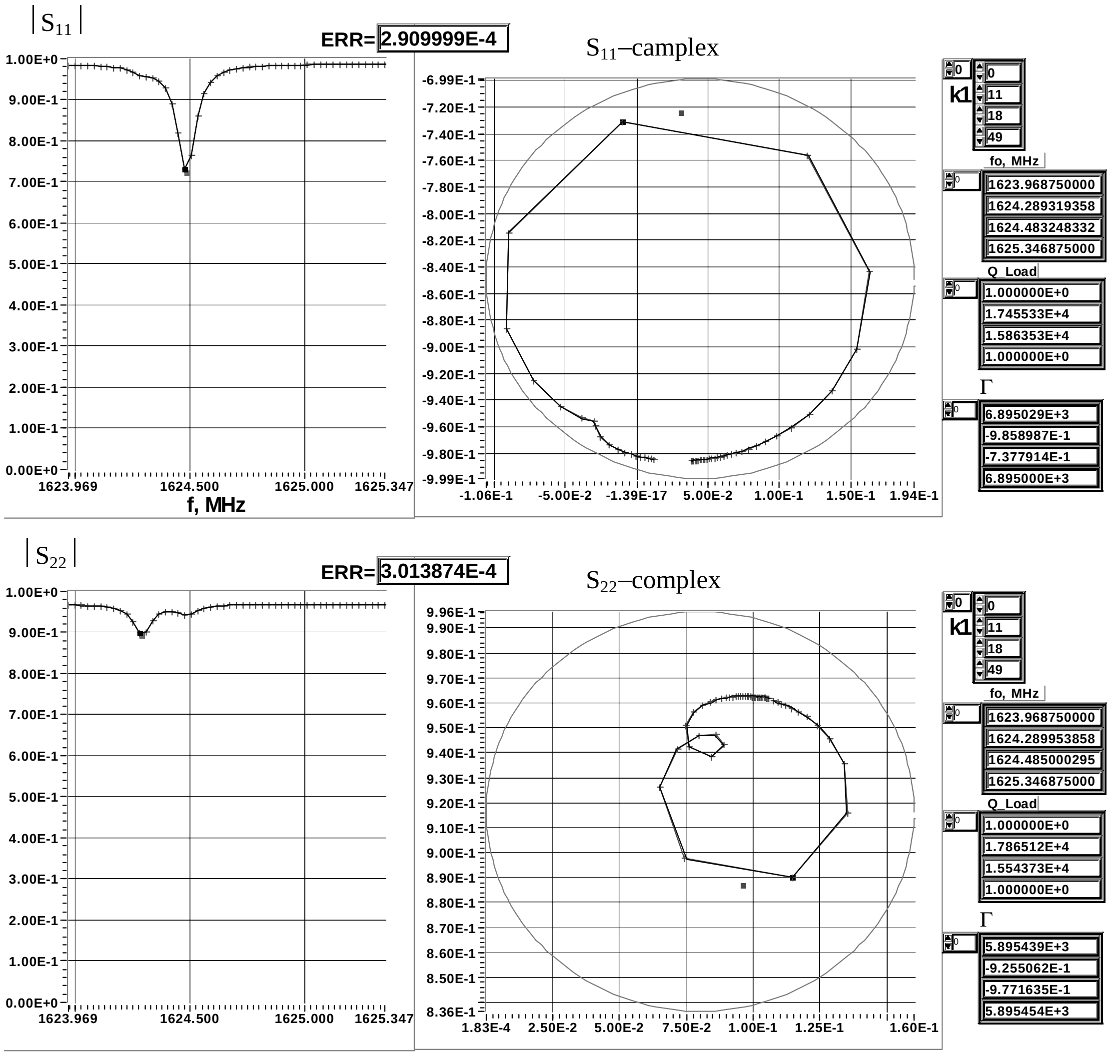

Fig.18 S_{11} and S_{22} dependence on frequency. First dipole band, first mode. Original–modified HOMCs.

The following table presents the calculation results obtained for this example. One can see that the modified downstream HOMC provides conditions for stronger suppression of both resonances (Q_{ext}=583180/398680 and 122080/110180).

	f_o, MHz	Q_{Load}	Q_o	Q_{ext}
original-original HOMCs ; S_{11}	1624.290	17510	18590	583180
	1624.488	16090	18540	122080
original-original HOMCs ; S_{22}	1624.288	18510	18590	583180
	1624.488	16090	18590	122080
original-modified HOMCs ; S_{11}	1624.289	17460	18480	398680
	1624.483	15860	18310	110180
original-modified HOMCs ; S_{22}	1624.290	17870	18480	398680
	1624.485	15540	18310	110180

Fig.19 and Fig.20 represent an example of a calculation in the frequency range containing three dipole modes (2^{nd}, 3^{rd} and 4^{th}) from the first dipole band. In this calculation we used 190 measured points (50 points cover the 2^{nd} dipole mode, 50 points cover the 3^{rd} dipole mode and 90 points cover the 4^{th} dipole mode). There are six resonances in this frequency range (three double resonances) corresponding to double polarization of each mode. Resonant frequencies, loaded Q-factors, Γ–values and error-function values are shown in Fig.19 and Fig.20 too. One can see good agreement between the measured (solid) and approximated (+) resonance curves.

Fig.21 shows external the Q-factor for the 2^{nd}, 3^{rd} and 4^{th} modes of the first dipole band and two combinations of HOMCs: the original-original HOMCs (black points) and original-modified HOMCs (white points). The first and second resonances correspond to the second dipole mode (double polarization); the third and fourth resonances correspond to the third dipole mode (double polarization); the fifth and sixth resonances correspond to the fourth dipole mode (double polarization).

One can see that the modified HOMC provides stronger suppression of resonances with higher Q_{ext} and only little increase in Q_{ext} for the resonances with lower Q_{ext}.

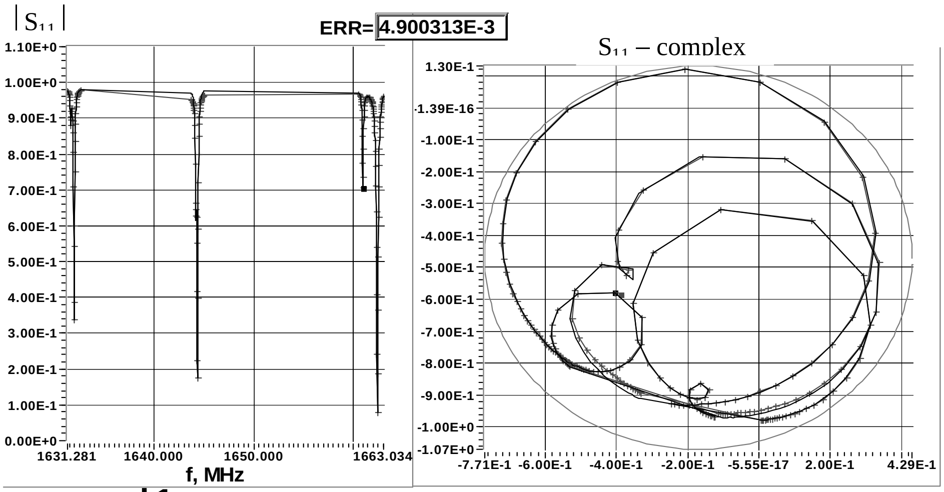

k1	fo, MHz	Q_Load	Γ
0	1631.281250000	1.000000E+0	4.397204E+2
12	1631.620823878	1.620018E+4	-9.147044E-1
24	1631.967832526	1.167797E+4	-3.243127E-1
68	1644.169006272	1.626007E+4	-7.736303E-1
75	1644.357769716	9.011463E+3	-1.815558E-1
115	1660.957714760	1.313290E+4	-7.313044E-1
167	1662.422643031	6.219048E+3	5.459557E-2
189	1663.034375000	1.000000E+0	4.395892E+2

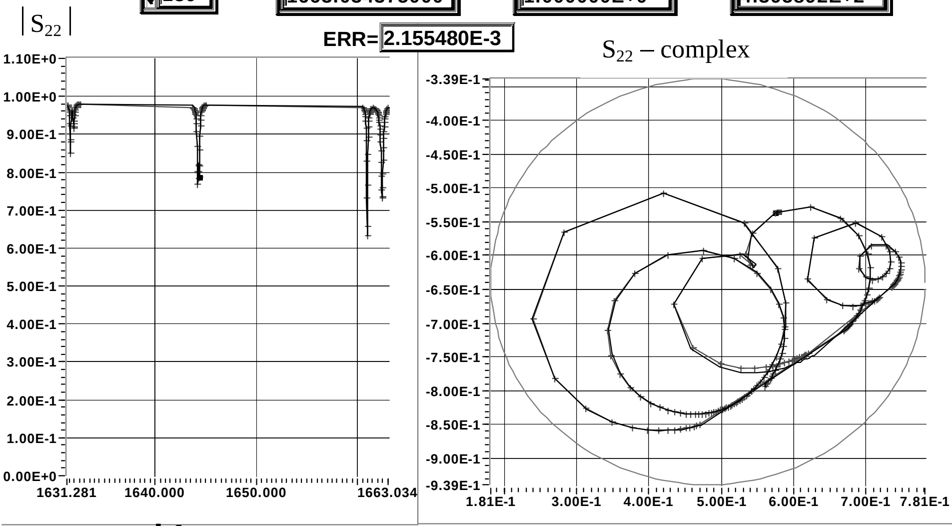

k1	fo, MHz	Q_Load	Γ
0	1631.281250000	1.000000E+0	3.305650E+2
12	1631.620578800	1.647347E+4	-8.735583E-1
24	1631.969216306	1.137296E+4	-9.357933E-1
68	1644.178026946	1.592931E+4	-8.423198E-1
75	1644.362277995	8.658463E+3	-8.205054E-1
115	1660.962102658	1.320268E+4	-6.463733E-1
167	1662.430244557	6.346498E+3	-7.512826E-1
189	1663.034375000	1.000000E+0	3.305124E+2

Fig.19 S_{11} and S_{22} dependence on frequency. First dipole band, 2^{nd}, 3^{rd}, 4^{th} modes. Original–original HOMCs.

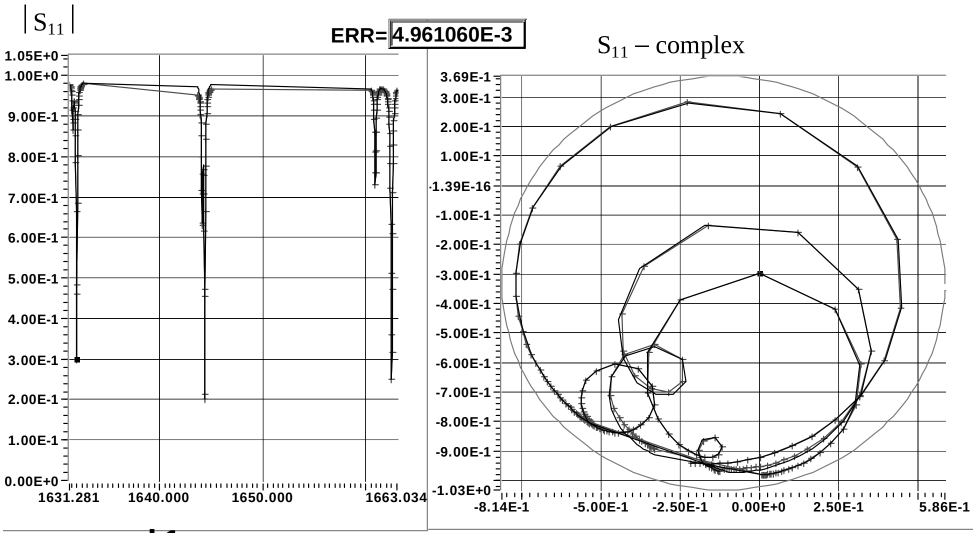

k1	fo, MHz	Q_Load	Γ
0	1631.281250000	1.000000E+0	4.390837E+2
12	1631.615429000	1.458957E+4	-8.946300E-1
25	1631.984181701	1.228523E+4	-3.123459E-1
68	1644.142961227	1.254402E+4	-6.903968E-1
77	1644.408022217	1.056761E+4	-1.528465E-1
114	1660.925247976	9.731784E+3	-7.561351E-1
170	1662.506470272	7.439834E+3	2.305947E-1
189	1663.034375000	1.000000E+0	4.388334E+2

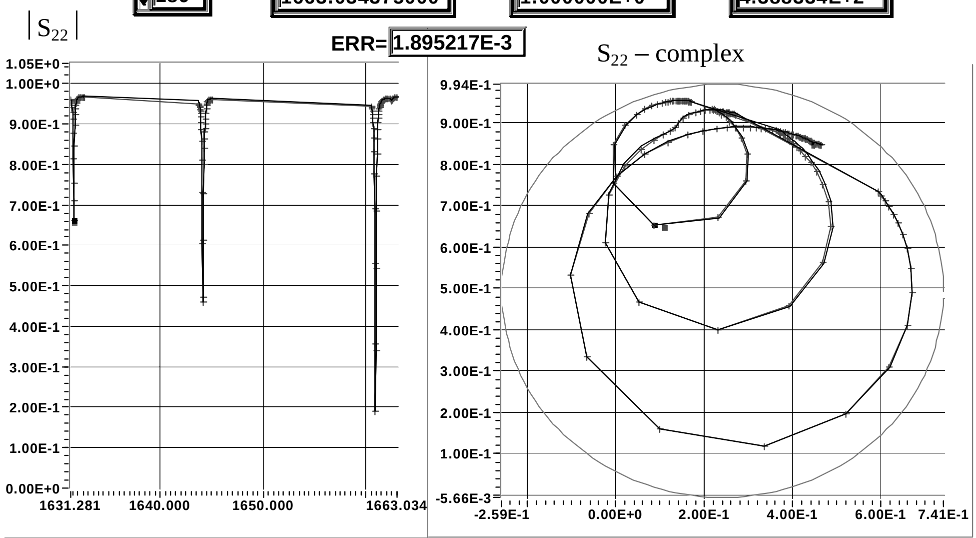

k1	fo, MHz	Q_Load	Γ
0	1631.281250000	1.000000E+0	3.608667E+2
12	1631.614315477	1.483213E+4	-6.874587E-1
25	1631.984181701	1.228523E+4	-9.993632E-1
67	1644.145450560	1.130224E+4	-4.879052E-1
77	1644.415262543	7.936237E+3	-9.639137E-1
114	1660.925980433	9.605635E+3	-2.223752E-1
170	1662.461322411	1.126353E+4	-9.918205E-1
189	1663.034375000	1.000000E+0	3.604737E+2

Fig.20 S_{11} and S_{22} dependence on frequency. First dipole band, 2nd, 3rd, 4th modes. Original–modified HOMCs.

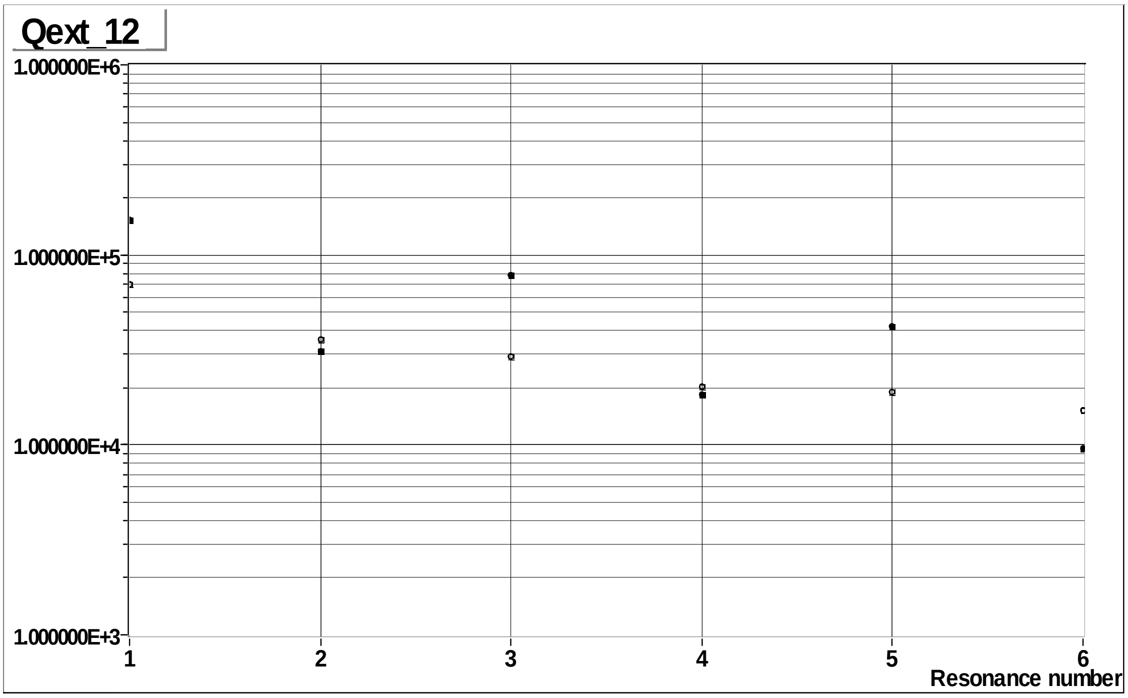

Fig.21 External Q-factor of 2nd, 3rd, 4th modes of first dipole band.
Black points → original − original HOMCs.
White points → original − modified HOMCs.

4.2 Investigation of the First, Second and Third Dipole Bands

Here we represent results for the first, second and third dipole bands for two cavities. We carried out an investigation of the cavity-coupler units equipped with original upstream and downstream HOMCs and with original upstream HOMC and modified ("mirrored") downstream HOMC. Measurements were carried out for two cavities and for six cavity rotation angles around cavity axis (0, 30, 60, 90, 120 and 150 degrees; HOMCs position is fixed).

Fig. 22 shows the resonant frequency as a function of mode number. Here the first 10 modes (1^{st} … 10^{th}) represent the first dipole band, the next 8 modes (11^{th} …18^{th}) represent the second dipole band and the last 6 modes (19^{th} … 24^{th}) represent the third dipole band. Two lower modes of the third dipole band and modes of the second quadrupole band overlap each other. Therefore these two modes are absent in Fig.22, 23 and 24 (see subsection 4.4).

The next six figures (Fig.23 a, b, c, d, e, f) show the external Q-factor dependence on mode number for six cavity-1 rotation angles around cavity axis and for two types of downstream HOMCs (original and modified). Here black points correspond to original upstream and downstream HOMCs and white points correspond to original upstream HOMC and modified ("mirrored") downstream HOMC. Two resonances or double polarization of dipole mode correspond to each mode number.

The following six figures (Fig.24 a, b, c, d, e, f) show the dependence of the external Q-factor on mode number for six cavity-2 rotation angles around cavity axis and for two types of downstream HOMCs (original and modified).

The most important modes with large (R/Q)-ratio are the 6th, 7th, 13th, 14th, 15th and 24th modes.

One can see that figures a, b, c, d, e, f look slightly different due to the circular asymmetry of the cavities and that the external Q-factor depends on the rotation angle of the cavity. In some cases (or rotation angle) the modified downstream HOMC provides very large suppression of the 24th mode with polarization corresponding to high external Q-factor and very little increase in the external Q-factor of the 24th mode with polarization corresponding to the low external Q-factor. In other cases the modified downstream HOMC changes the external Q-factor very little. So if the original upstream and downstream HOMCs have strong coupling with both polarizations of the 24th mode then the modified downstream HOMC changes the external Q-factor very little. However if the original upstream and downstream HOMCs have strong coupling with one polarization of the 24th mode and weak coupling with the other polarization, then the modified downstream HOMC provides very large suppression of the 24th mode with polarization corresponding to high external Q-factor and very little increase in the external Q-factor of the 24th mode with polarization corresponding to low external Q-factor.

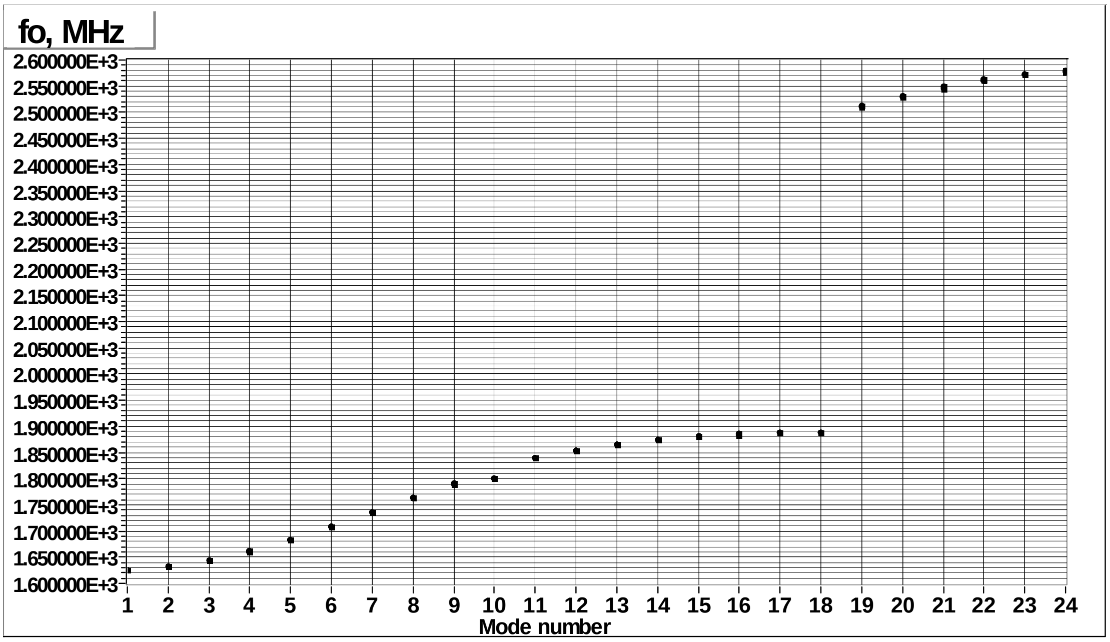

Fig.22.Frequency of modes.
1st – 10th modes correspond to the first dipole band;
11th – 18th modes correspond to the second dipole band;
19th – 24th modes correspond to the third dipole band (six upper modes of eight modes).

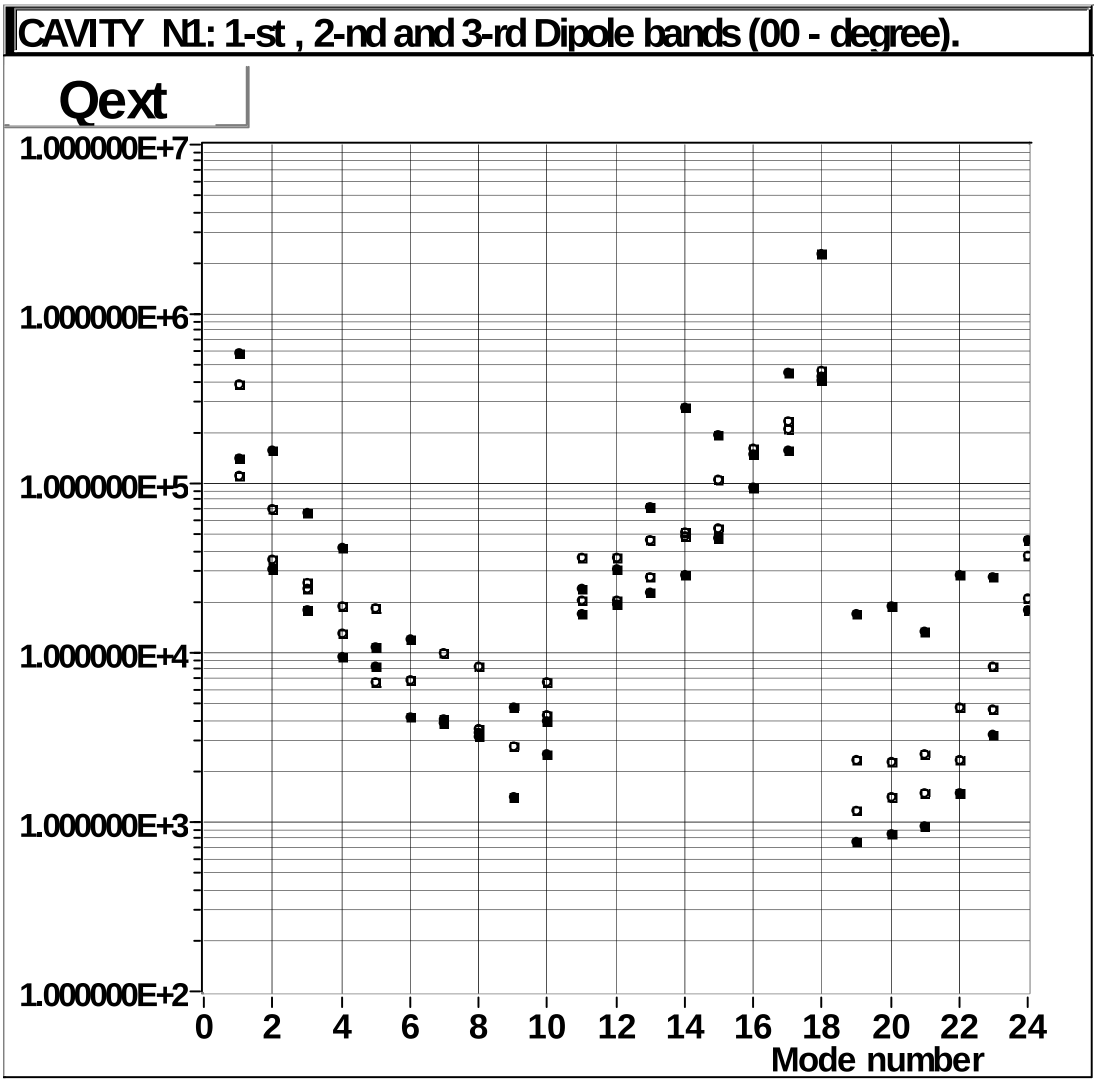

CAVITY N1: 1-st , 2-nd and 3-rd Dipole bands (00 - degree).
Qext
1.000000E+7
1.000000E+6
1.000000E+5
1.000000E+4
1.000000E+3
1.000000E+2
0
2
4
6
8
10
12
14
16
18
20
22
24
Mode number

Fig.23 a

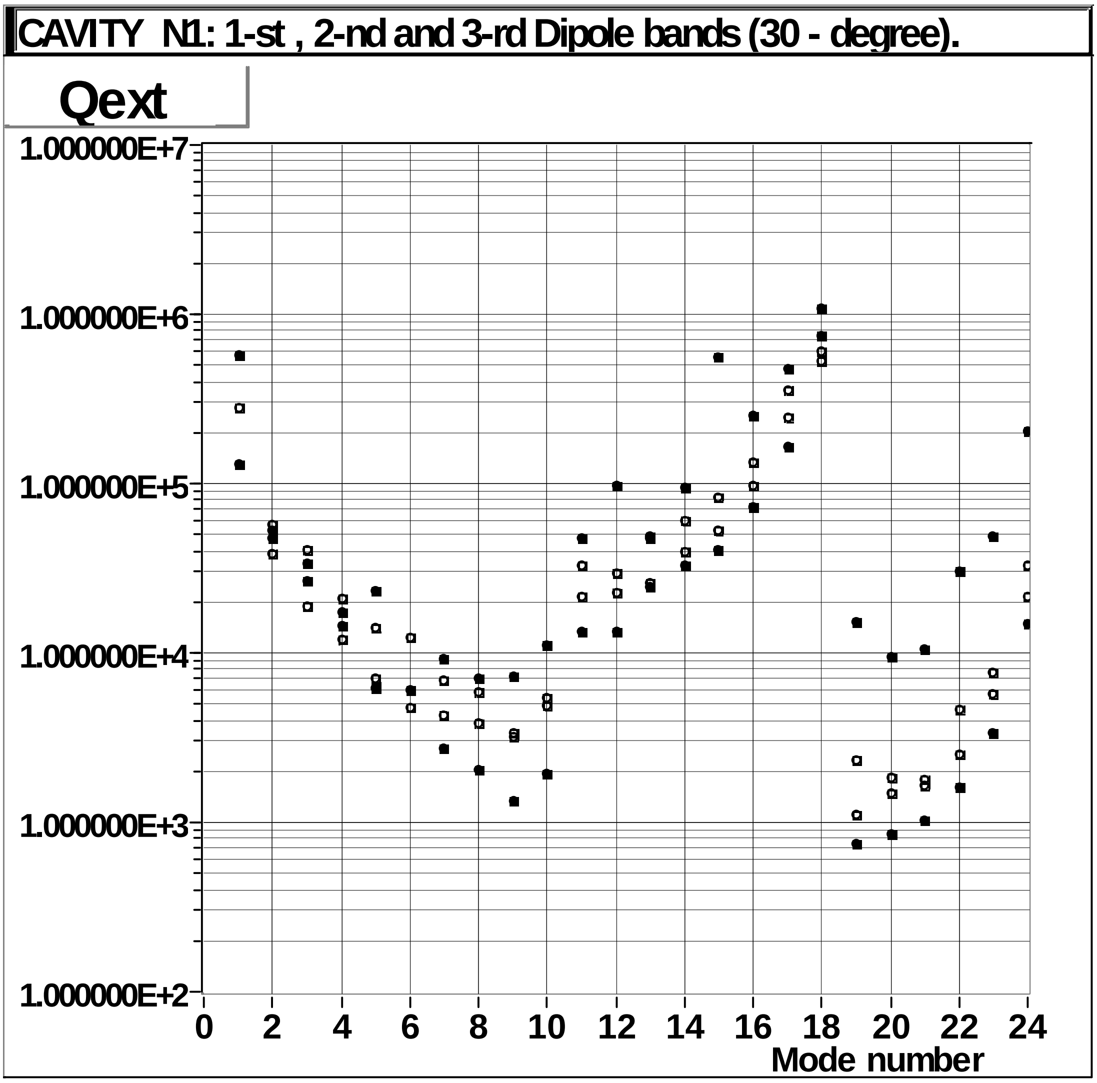
CAVITY N1: 1-st , 2-nd and 3-rd Dipole bands (30 - degree).
Qext
1.000000E+7
1.000000E+6
1.000000E+5
1.000000E+4
1.000000E+3
1.000000E+2
0 2 4 6 8 10 12 14 16 18 20 22 24
Mode number

Fig.23 b

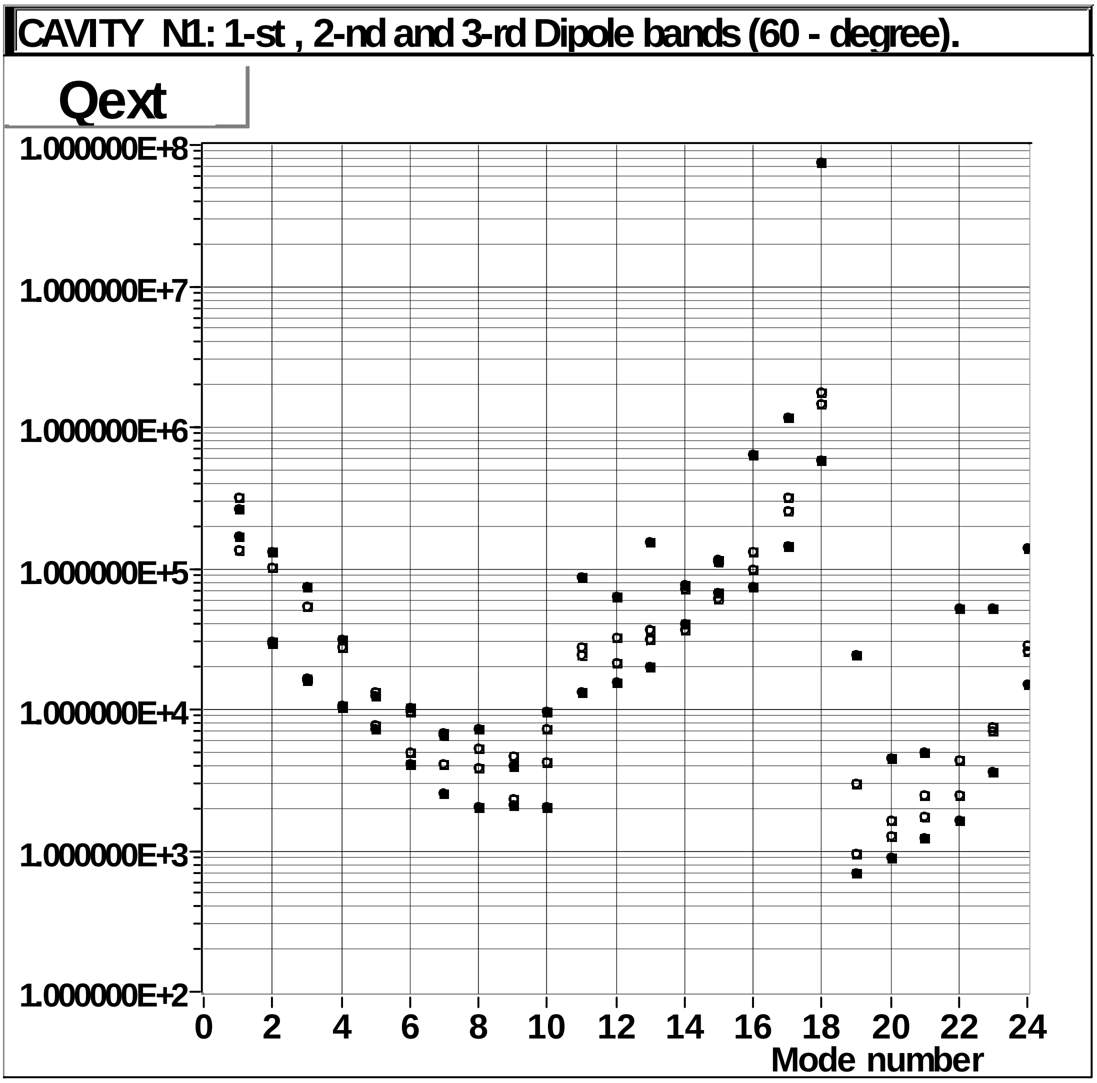
CAVITY N1: 1-st , 2-nd and 3-rd Dipole bands (60 - degree).
Qext
1.000000E+8
1.000000E+7
1.000000E+6
1.000000E+5
1.000000E+4
1.000000E+3
1.000000E+2
0 2 4 6 8 10 12 14 16 18 20 22 24
Mode number

Fig.23 c

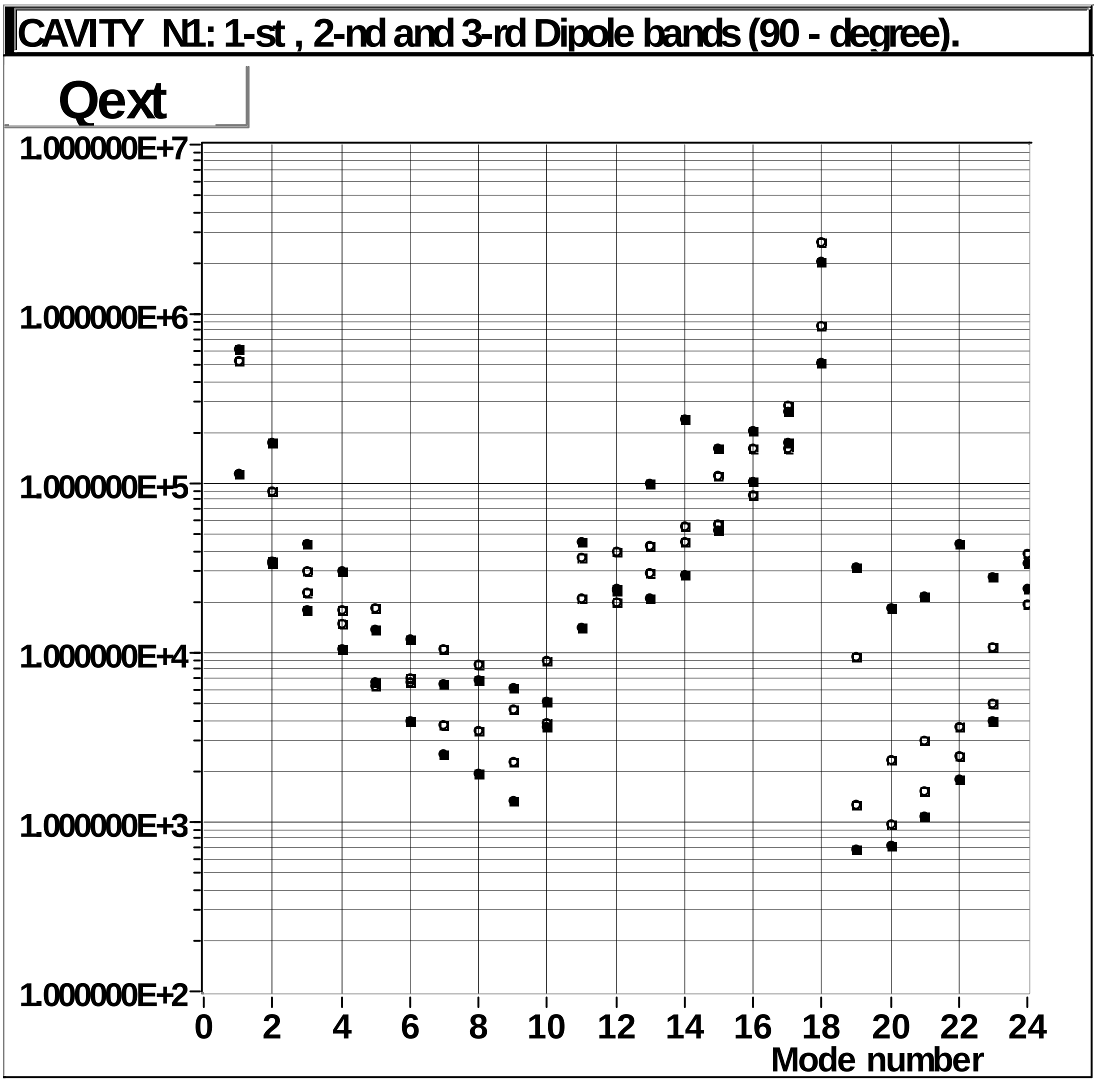
CAVITY N1: 1-st , 2-nd and 3-rd Dipole bands (90 - degree).
Qext
1.000000E+7
1.000000E+6
1.000000E+5
1.000000E+4
1.000000E+3
1.000000E+2
0 2 4 6 8 10 12 14 16 18 20 22 24
Mode number

Fig.23 d

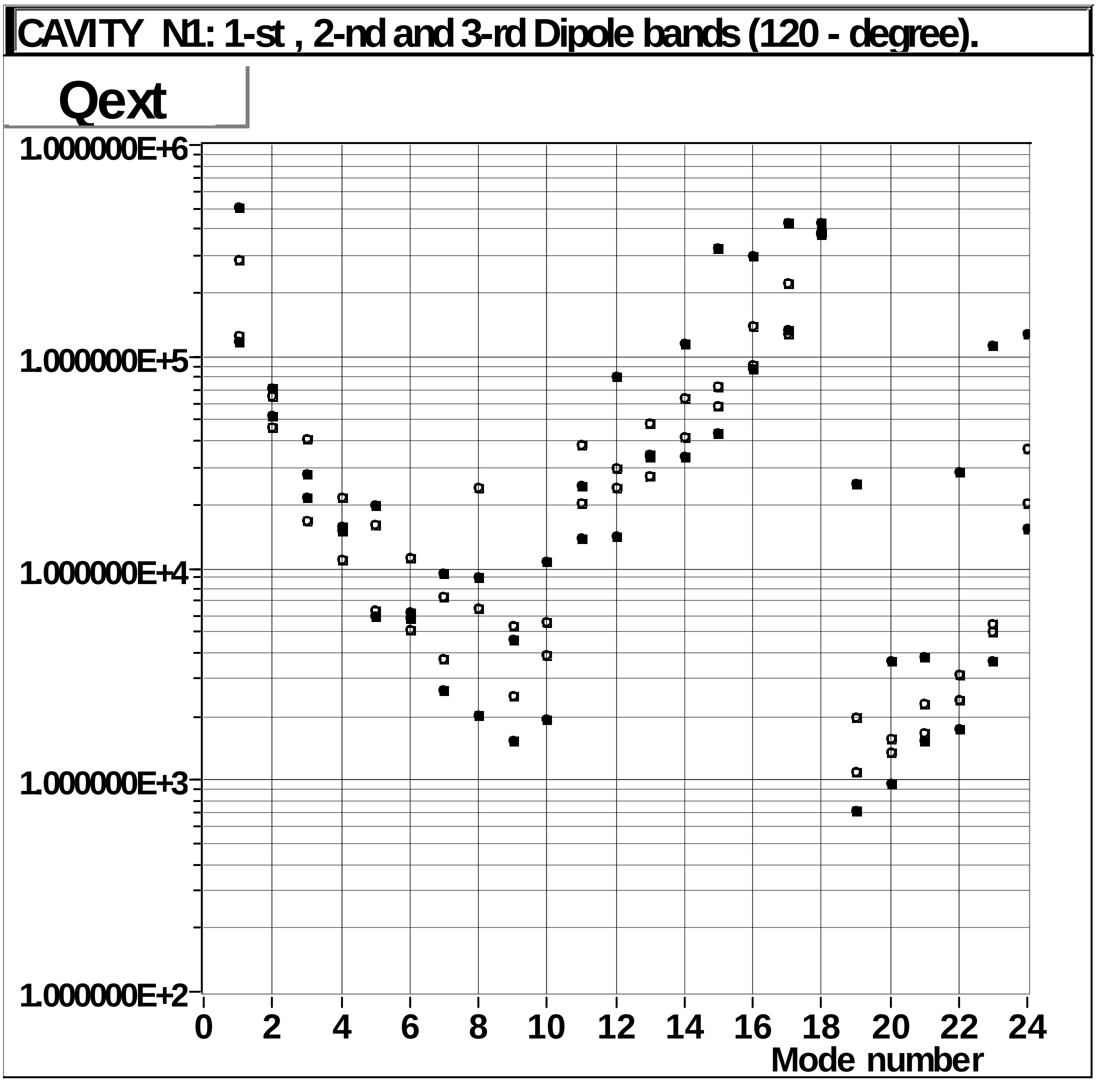

CAVITY N1: 1-st , 2-nd and 3-rd Dipole bands (120 - degree).
Qext
1.000000E+6
1.000000E+5
1.000000E+4
1.000000E+3
1.000000E+2
0
2
4
6
8
10
12
14
16
18
20
22
24
Mode number

Fig.23 e

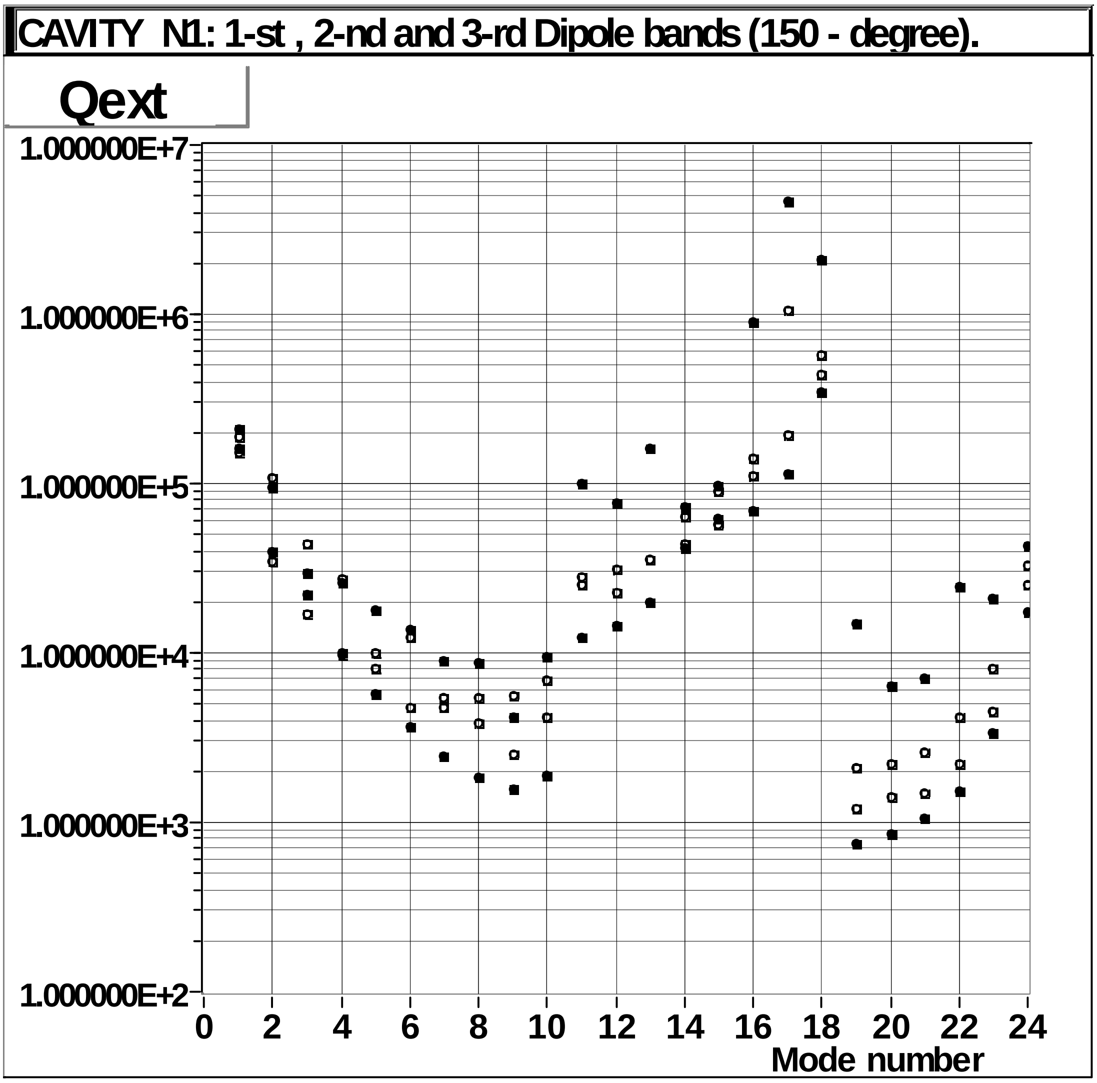
CAVITY N1: 1-st , 2-nd and 3-rd Dipole bands (150 - degree).
Qext
1.000000E+7
1.000000E+6
1.000000E+5
1.000000E+4
1.000000E+3
1.000000E+2
0 2 4 6 8 10 12 14 16 18 20 22 24
Mode number

Fig.23 f

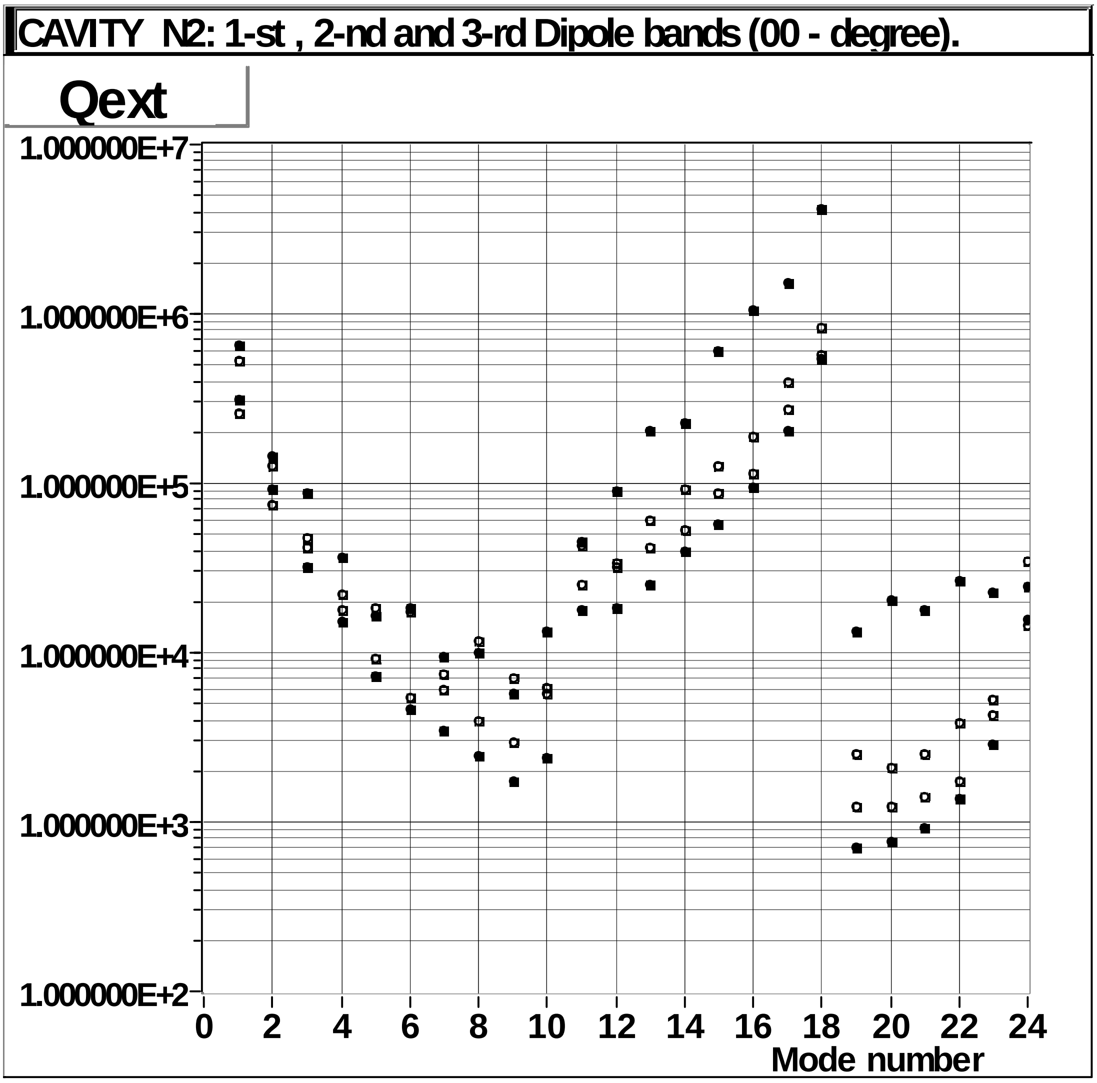

CAVITY N2: 1-st , 2-nd and 3-rd Dipole bands (00 - degree).
Qext
1.000000E+7
1.000000E+6
1.000000E+5
1.000000E+4
1.000000E+3
1.000000E+2
0
2
4
6
8
10
12
14
16
18
20
22
24
Mode number

Fig.24 a

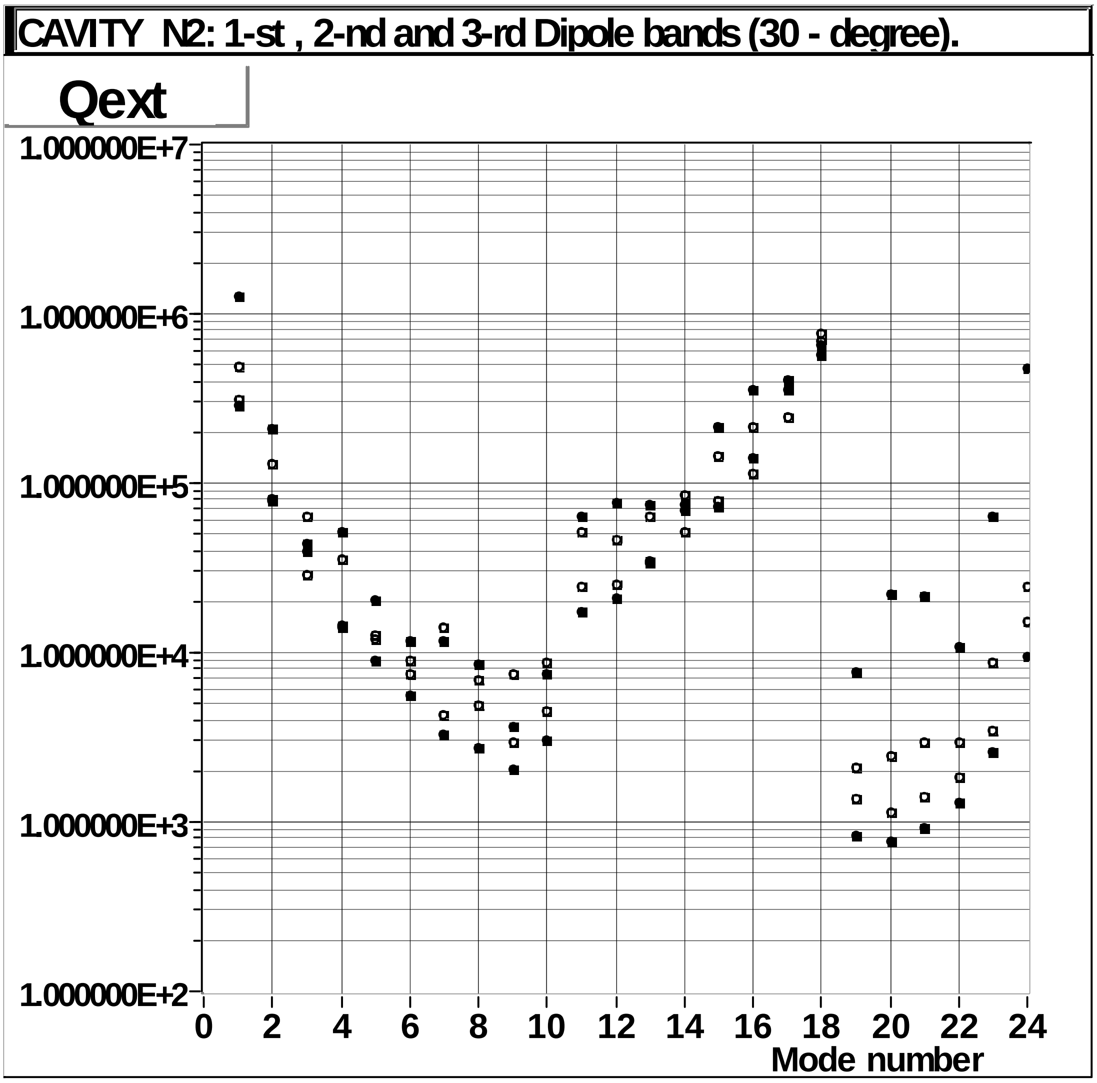
CAVITY N2: 1-st , 2-nd and 3-rd Dipole bands (30 - degree).
Qext
1.000000E+7
1.000000E+6
1.000000E+5
1.000000E+4
1.000000E+3
1.000000E+2
0
2
4
6
8
10
12
14
16
18
20
22
24
Mode number

Fig.24 b

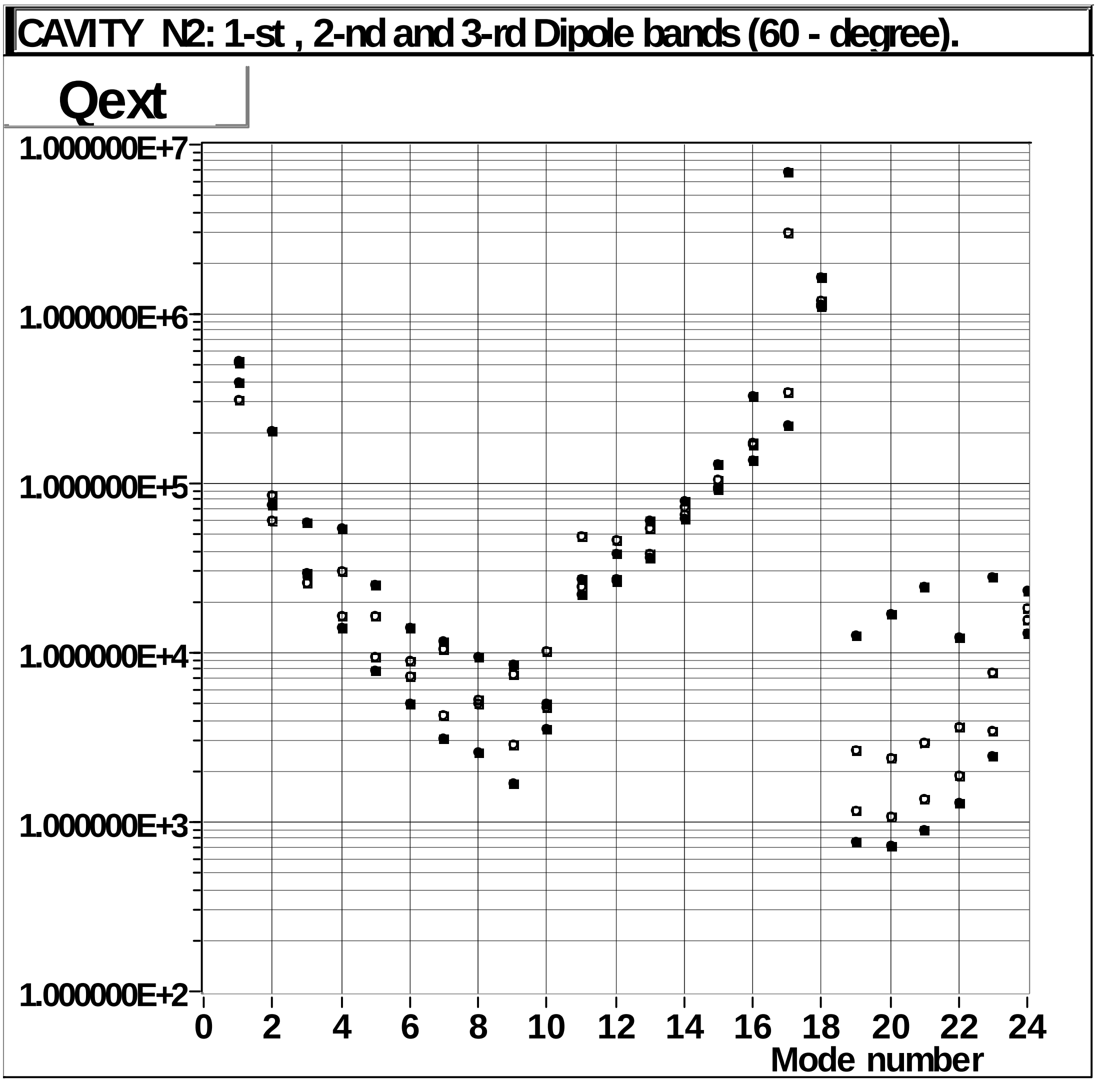
CAVITY N2: 1-st , 2-nd and 3-rd Dipole bands (60 - degree).
Qext
1.000000E+7
1.000000E+6
1.000000E+5
1.000000E+4
1.000000E+3
1.000000E+2
0
2
4
6
8
10
12
14
16
18
20
22
24
Mode number

Fig.24 c

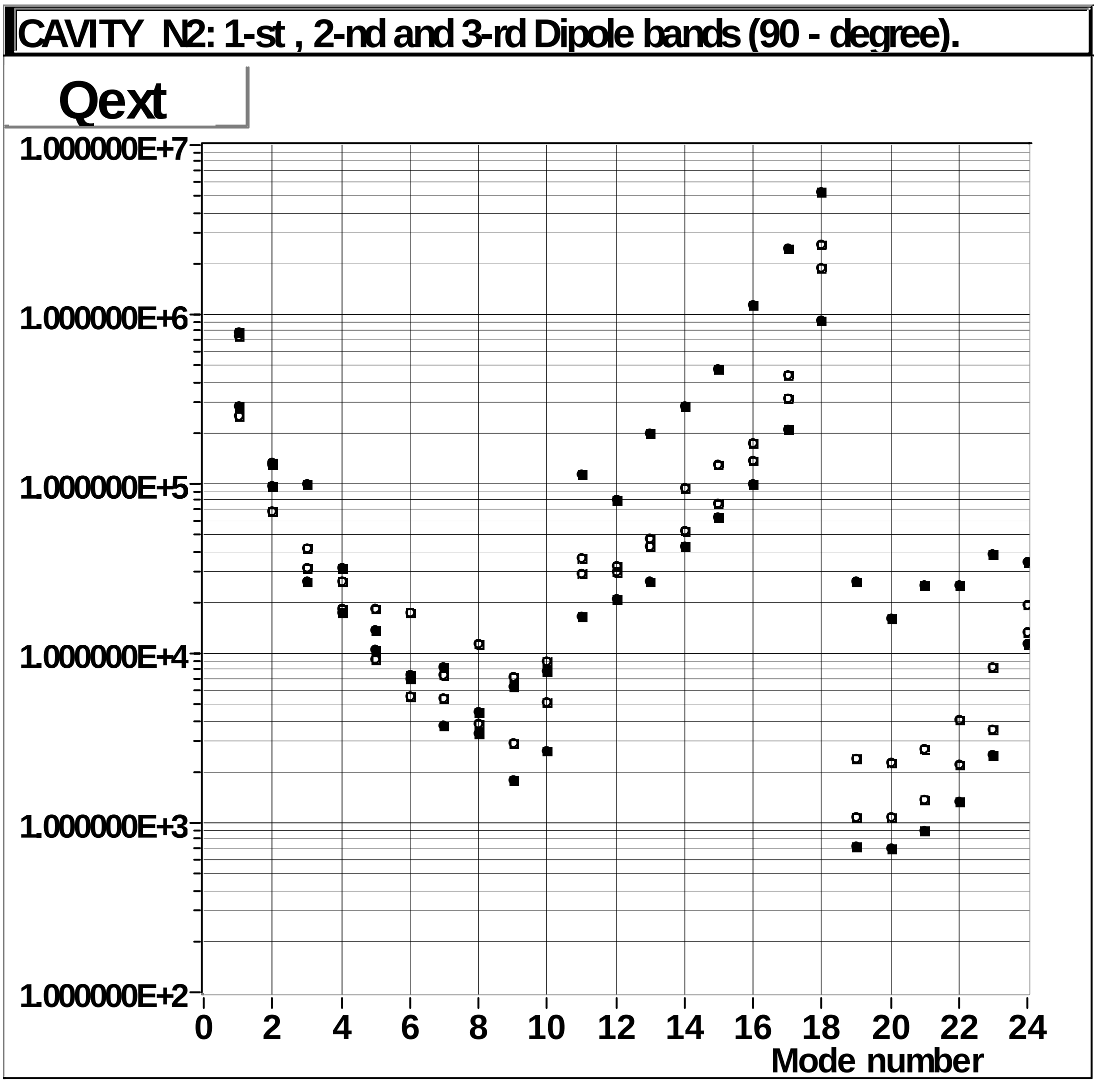
CAVITY N2: 1-st , 2-nd and 3-rd Dipole bands (90 - degree).
Qext
1.000000E+7
1.000000E+6
1.000000E+5
1.000000E+4
1.000000E+3
1.000000E+2
0 2 4 6 8 10 12 14 16 18 20 22 24
Mode number

Fig.24 d

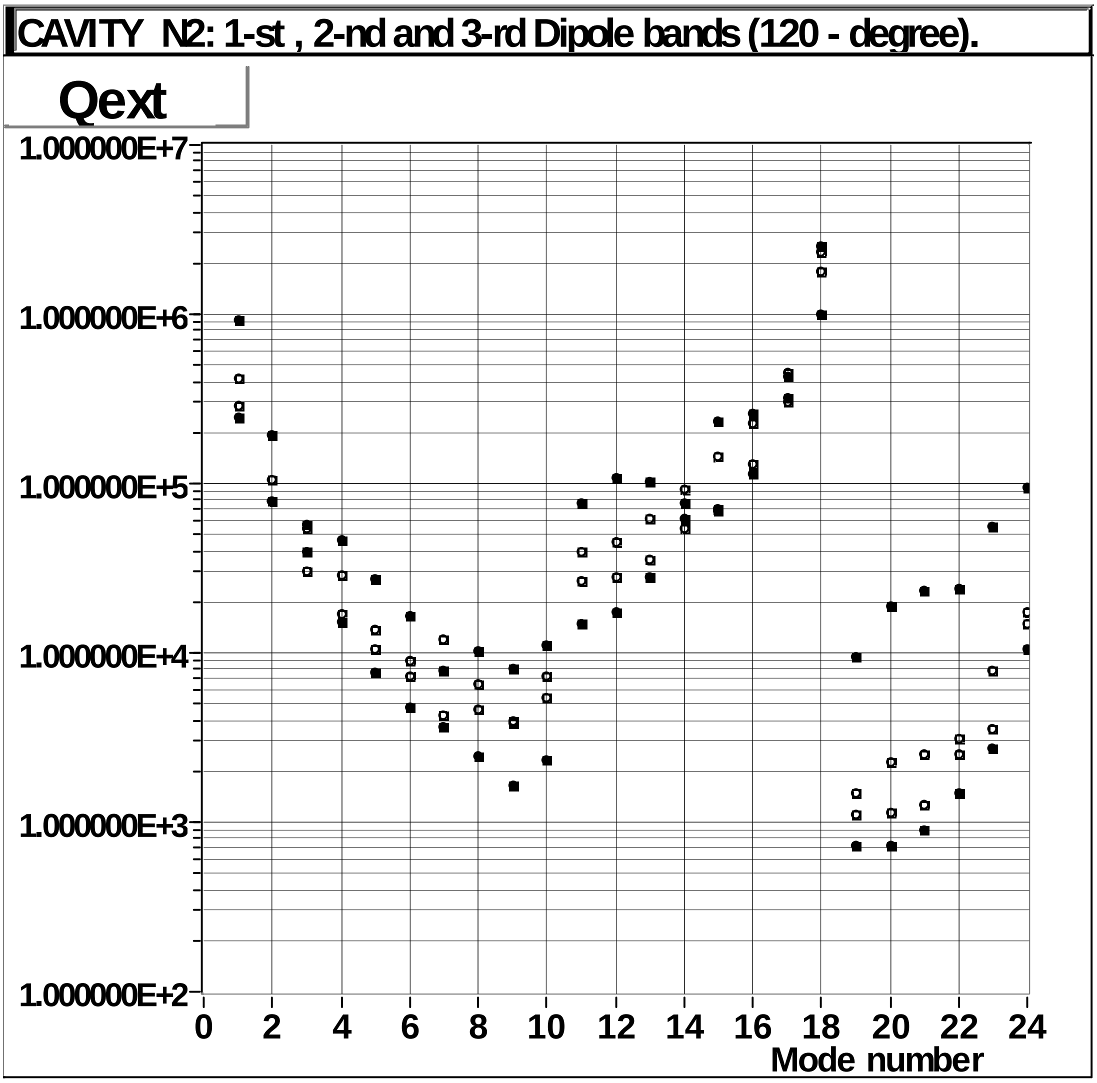
CAVITY N2: 1-st , 2-nd and 3-rd Dipole bands (120 - degree).
Qext
1.000000E+7
1.000000E+6
1.000000E+5
1.000000E+4
1.000000E+3
1.000000E+2
0 2 4 6 8 10 12 14 16 18 20 22 24
Mode number

Fig.24 e

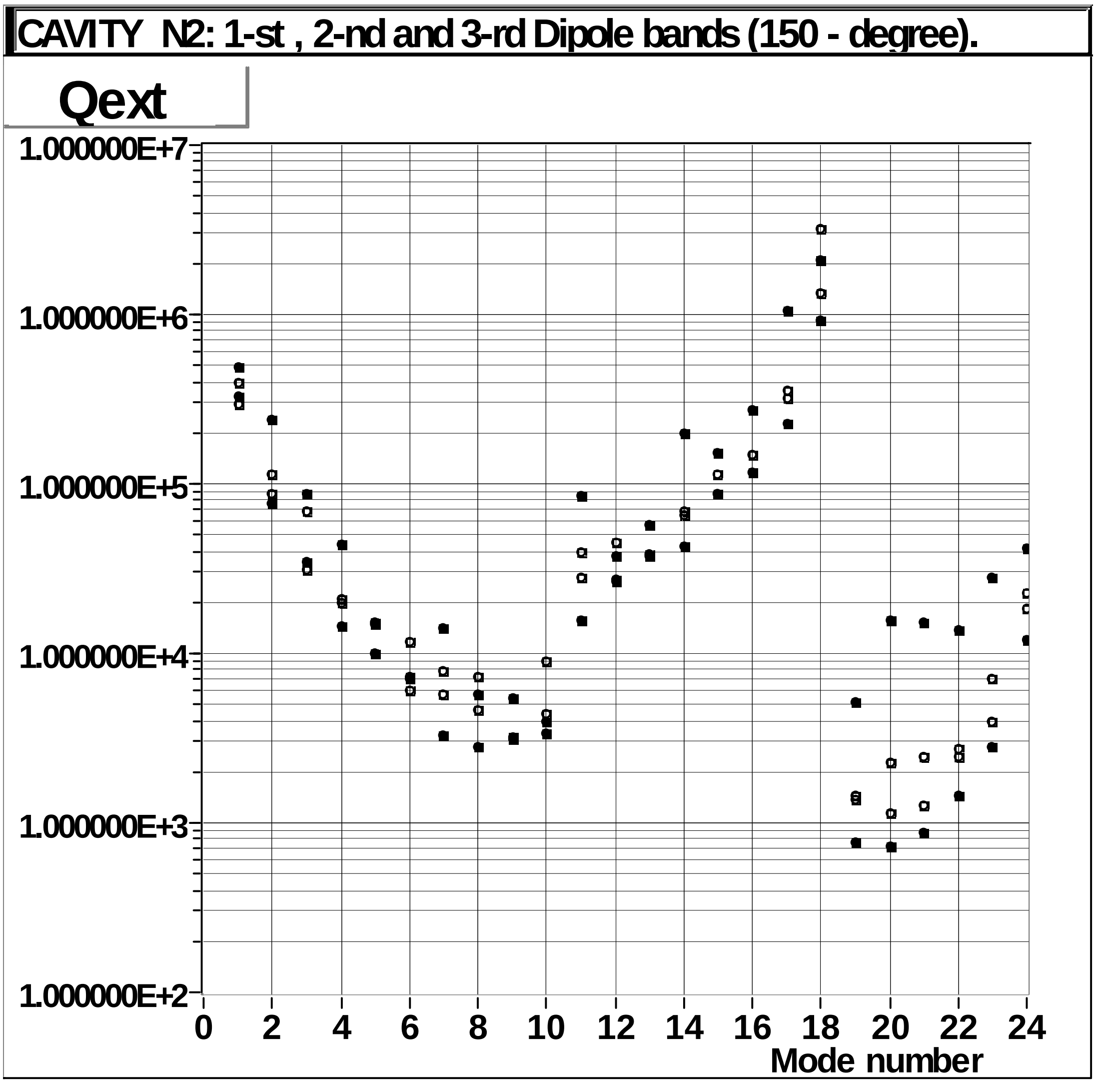

Fig.24 f

Other modes of the 3rd dipole band are suppressed more effectively by the modified downstream HOMC.

The 6th and 7th modes (these modes belong to the first dipole band) have low external Q-factors. One can see that the modified downstream HOMC provides more effective suppression of the 13th, 14th and 15th modes (these modes belong to the 2nd dipole band).

4.3 Investigation of the Second Monopole Band

Fig.25 shows the dependence of the external Q-factor on mode number for the second monopole band (seven upper modes of nine, there is no double polarization). Here black points correspond to original upstream and downstream HOMCs and white points correspond to original upstream HOMC and modified ("mirrored") downstream HOMC. One can see that modified ("mirrored") downstream HOMC changes external Q-factor very little. This is because the mirror modification of the downstream HOMC is not perfect. There is no change in external Q-factor in the case of a perfect mirror modification of the downstream HOMC.

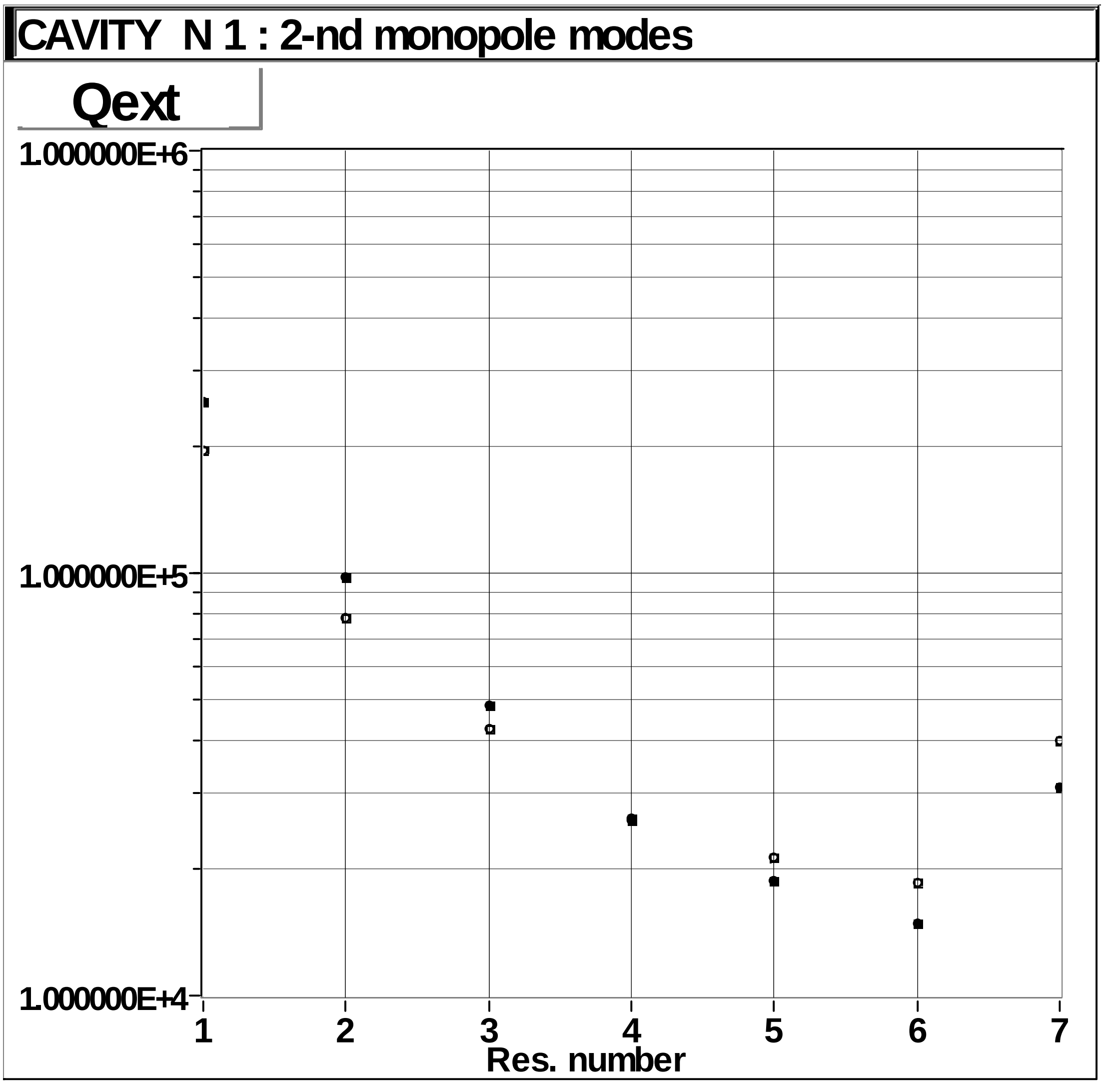

Fig.25 External Q-factor dependence on mode number for the second monopole band (7 upper modes of 9).

The most important modes are the 5th, 6th and 7th modes. One can see that external Q-factor is not very large for these modes.

4.4 Example of the Mutually Overlapping Second Quadrupole and Third Dipole Modes

Fig.26, 27 show the S_{11} and S_{22} dependence on frequency for the cavity-coupler unit with original upstream and downstream HOMCs. Fig.28, 29 show the similar curves for the cavity-coupler unit with original upstream and modified downstream HOMCs. The frequency range covers some modes from the second quadrupole band and one mode from the third dipole band (there are seven resonances in this frequency range). One can see good agreement between the measured (solid) and approximated (+) resonance curves.

In both cases the upstream HOMC sees the first resonance mode and does not see the last resonance mode, but the downstream HOMC sees the last resonance mode and does not see the first resonance mode.

Fig.30 shows the external Q-factors of the second quadrupole modes and the first mode of the third dipole band.

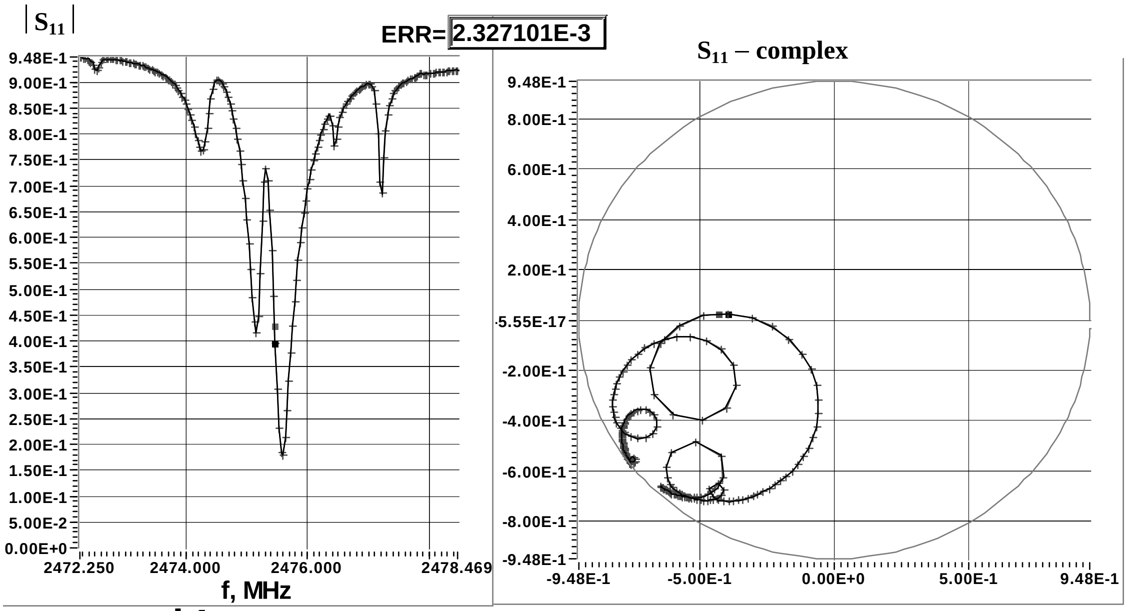

K1	fo, MHz	Q_Load	Γ
0	2472.250000000	1.000000E+0	4.945125E+3
9	2472.545031328	1.975601E+4	-9.713957E-1
66	2474.330318696	7.586923E+3	-8.074003E-1
96	2475.252714878	9.185110E+3	-2.187352E-1
103	2475.457202865	3.355889E+3	1.676823E-1
134	2476.429372207	2.808200E+4	-9.193484E-1
158	2477.196768866	2.149828E+4	-7.666439E-1
179	2477.846481030	3.715601E+4	-9.942443E-1
199	2478.468750000	1.000000E+0	4.944327E+3

Fig.26 S_{11} dependence on frequency. Original-original HOMCs.

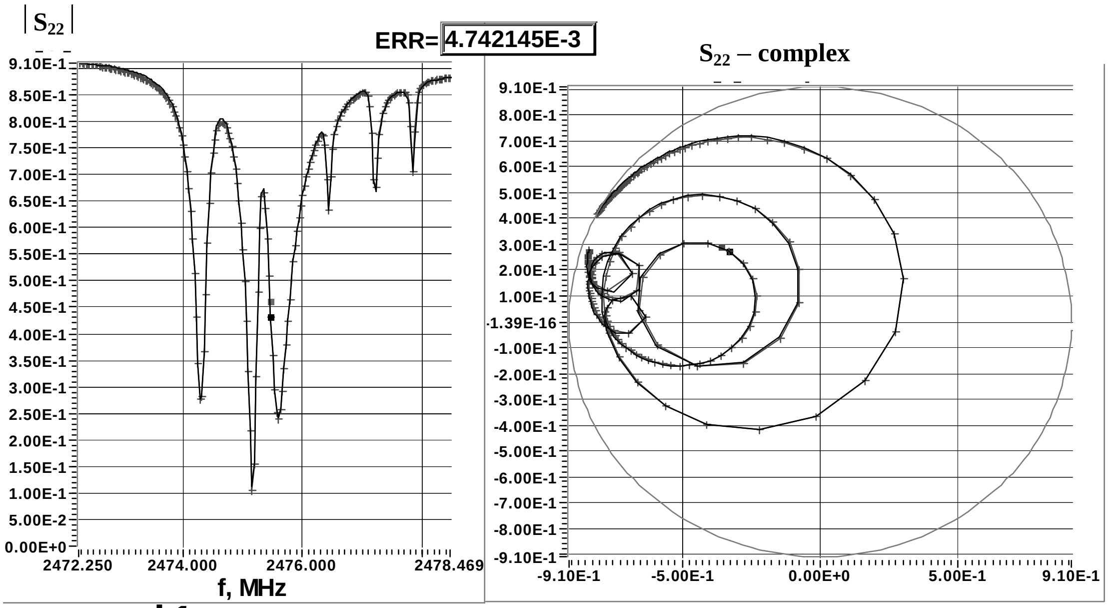

K1	fo, MHz	Q_Load	Γ
0	2472.250000000	1.000000E+0	1.019724E+4
9	2472.544507986	1.979885E+4	-9.979091E-1
66	2474.320662409	7.717676E+3	2.279172E-1
96	2475.243849971	8.834020E+3	1.527436E-1
103	2475.457115744	3.591268E+3	2.244551E-1
134	2476.427614301	2.848890E+4	-8.249294E-1
158	2477.193660466	2.242158E+4	-7.974301E-1
179	2477.846481030	3.715601E+4	-8.350592E-1
199	2478.468750000	1.000000E+0	1.019779E+4

Fig.27 S_{22} dependence on frequency. Original-original HOMCs.

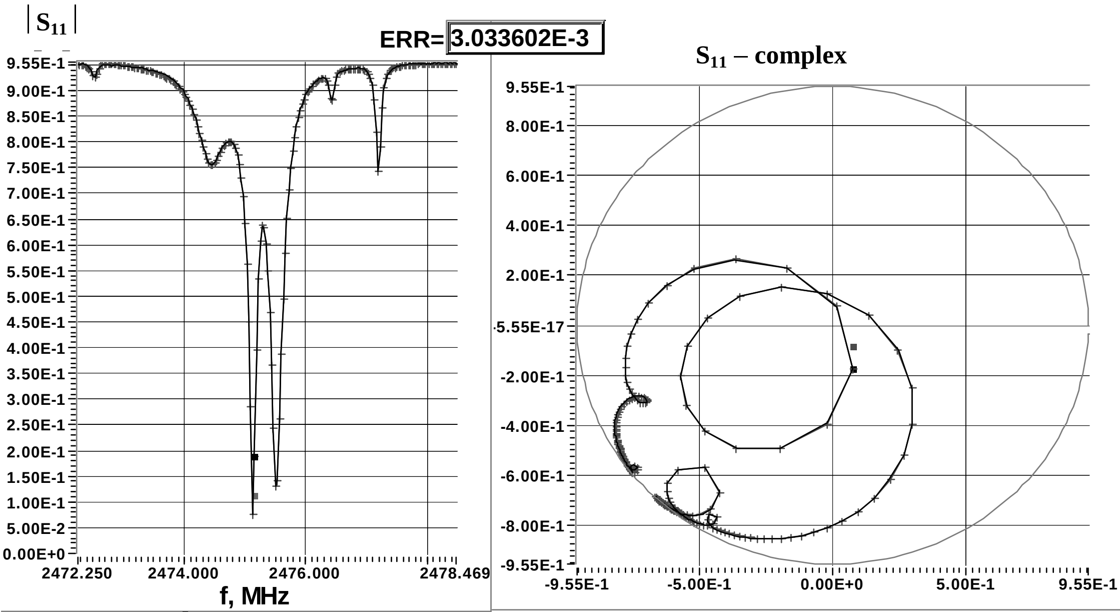

k1	fo, MHz	Q_Load	Γ
0	2472.250000000	1.000000E+0	5.724988E+3
9	2472.545580578	1.936601E+4	-9.696106E-1
69	2474.432224228	4.217608E+3	-8.169452E-1
93	2475.145695718	1.164499E+4	4.188709E-2
104	2475.512376572	6.657143E+3	2.115239E-1
134	2476.426387613	3.083933E+4	-9.382395E-1
158	2477.192714116	2.497663E+4	-7.884488E-1
179	2477.846481030	3.715601E+4	-9.964256E-1
199	2478.468750000	1.000000E+0	5.723954E+3

Fig.28 S_{11} dependence on frequency. Original-modified HOMCs.

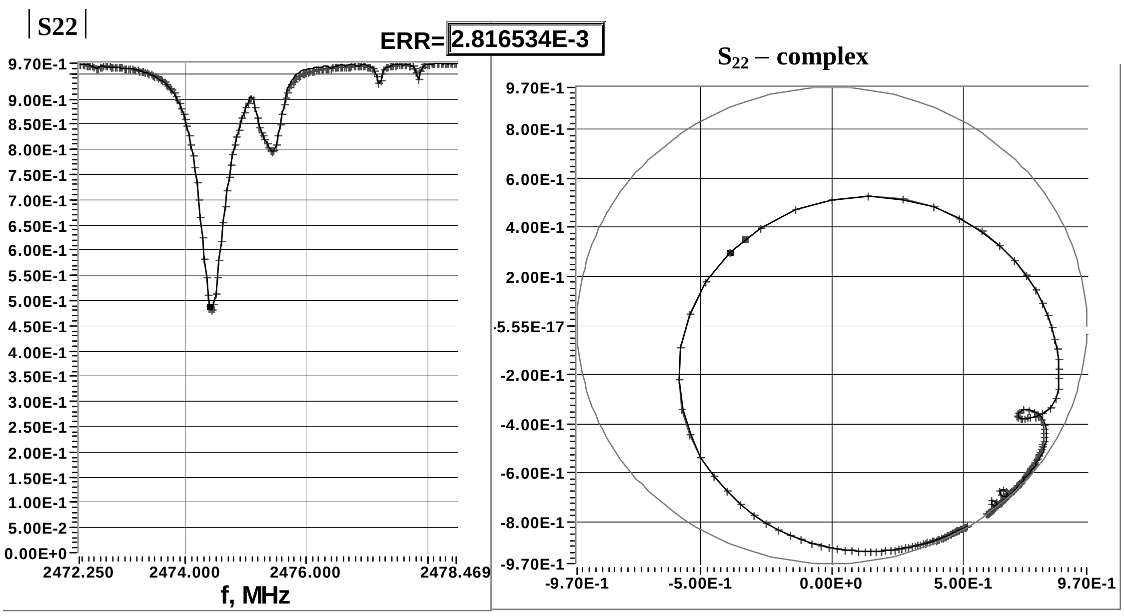

K1	fo, MHz	Q_Load	Γ
0	2472.250000000	1.000000E+0	9.225869E+3
9	2472.545580578	1.936601E+4	-9.944700E-1
69	2474.422243682	4.161702E+3	4.735767E-1
92	2475.156127459	1.252343E+4	-9.276830E-1
104	2475.492778942	7.200755E+3	-8.630982E-1
134	2476.825882145	8.342401E+1	-5.318379E-1
158	2477.195010352	2.384175E+4	-9.634773E-1
179	2477.845940916	3.493090E+4	-9.704343E-1
199	2478.468750000	1.000000E+0	9.227928E+3

Fig.29 S_{22} dependence on frequency. Original-modified HOMCs.

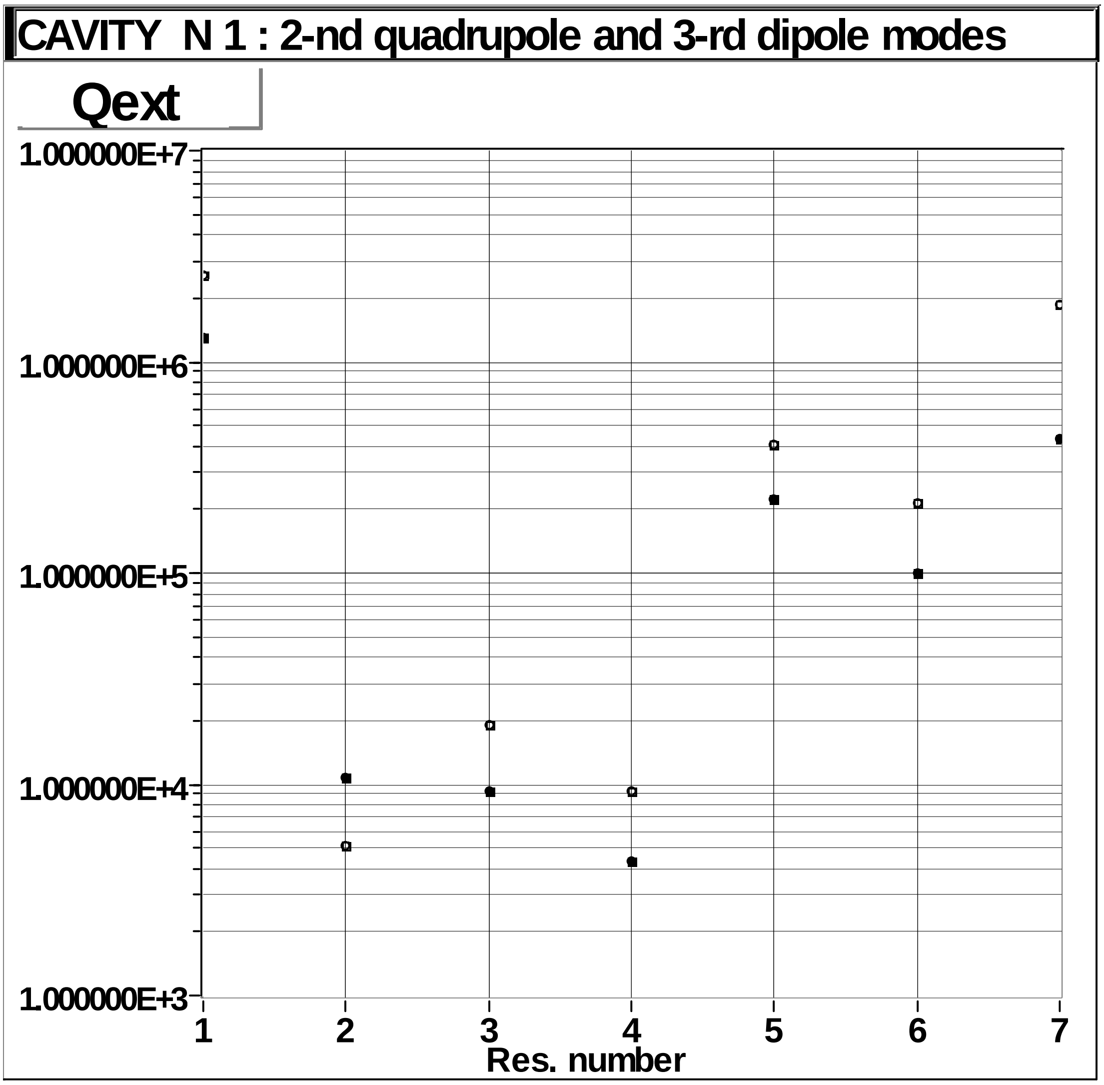

Fig.30 External Q-factor of second quadrupole modes and first mode of the third dipole band.

5. Conclusion

Resonant frequencies and Q-factors were calculated for complex multi-resonance lossless electrodynamic systems with multiple overlapping resonances. The procedure uses the dependence of the complex transmission coefficient, $S_{i,j}(f)$, on frequency in the frequency band under investigation and permits us to determine resonant frequencies and Q-factors using a frequency step Δf more than 3 dB band of the resonance system under investigation and only few frequency points located on the resonance curve corresponding to the high Q-factor resonance.

Experimental investigation of one cavity-coupler unit, consisting of a 9-cell TTF copper cavity and two (upstream and downstream) DESY-type HOMCs, was carried out to check a proposal presented in [4,5] to improve on the original HOMC and provide conditions for damping modes in the frequency range of the 3rd dipole band. We carried out an investigation of a cavity-coupler unit equipped with original upstream and downstream HOMCs and with original upstream HOMC and modified ("mirrored") downstream HOMC. The procedure for calculating resonant frequencies and Q-factors (f_o, Q_{Load}, Q_o, Q_{ext}) uses complex reflection coefficients $S_{11}(f)$ and $S_{22}(f)$ measured as a function of frequency.

It was shown that in some cases (certain rotation angles of cavity) the modified downstream HOMC provides a very good suppression of the 24th mode (the highest mode of the 3rd dipole band) with polarization corresponding to high external Q-factor and very little increasing in external Q-factor of the 24th mode with polarization corresponding to a low external Q-factor. In other cases the modified downstream HOMC changes the external Q-factor very little. So, if the original upstream and downstream HOMCs have strong coupling with both polarizations of the 24th mode, then the modified downstream HOMC changes the external Q-factor very little and if the original upstream and downstream HOMCs have strong coupling with one polarization of the 24th mode and weak coupling with the other polarization then the modified downstream HOMC provides very good suppression of the 24th mode with polarization corresponding to high external Q-factor and very little increase in the external Q-factor of the 24th mode with polarization corresponding to a low external Q-factor.

Investigation of the second monopole band shows that the modified ("mirrored") downstream HOMC changes the external Q-factor very little. This is because the mirror modification of downstream HOMC is not perfect. There is no change in external Q-factor in the case of perfect mirror modification of the downstream HOMC. The most important modes of this band do not have very large external Q-factor.

Investigation of mutually overlapping modes of the second quadrupole and third dipole bands is also presented here.

6. References

[1] D.A. Edwards (ed.): TESLA Test Facility Linac - Design Report, DESY TESLA-95-01, 1995.

[2] R. Brinkmann, G. Materlik, J. Rossbach and A. Wagener (eds.): Conceptual Design of a 500 GeV e+e- Collider with Integrated X-ray Laser Facility, DESY-97-048 and ECFA-97-182.

[3] R. Brinkmann, K. Flöttmann, J. Rossbach, P. Schmüser, N. Walker, H. Weise (eds.): TESLA The Superconducting Electron-Positron Linear Collider with an Integrated X-Ray Laser Laboratory, Technical Design Report, Part II The Accelerator, DESY 2001-011, ECFA 2001-209, TESLA Report 2001-23, TESLA-FEL 2001-05.

[4] M. Dohlus, V. Kaljuzhny, S.G. Wipf : Higher Order Mode Absorption in TTF Modules in the Frequency Range of the 3-rd Dipole Band, Proceedings of EPAC 2002, Paris, France, pp 1473-1475, TESLA Report 2002-05.

[5] D. Hecht, K. Rothemund, H.-W. Glock, U. van Rienen: Computation of RF-properties of Long and Complex Structures, Proceedings of EPAC 2002, Paris, France, pp 1685-1687.